

Contents lists available at ScienceDirect

Petroleum Science

journal homepage: www.keaipublishing.com/en/journals/petroleum-science



Original Paper

Oilfield sustainability and management: An optimization model for the reconstruction of oil and gas gathering systems based on potential location mining



Jie Chen, Wei Wang *, Wen-Yuan Sun, Dong Li, Yu-Bo Jiao

National Engineering Laboratory for Pipeline Safety/ MOE Key Laboratory of Petroleum Engineering, China University of Petroleum (Beijing), Beijing, 102249, China

ARTICLE INFO

Article history: Received 29 February 2024 Received in revised form 10 December 2024 Accepted 11 December 2024 Available online 18 December 2024

Edited by Jia-Jia Fei

Keywords:
Oilfield reconstruction
Sustainable development
Optimization model
Potential location
3-phase heuristic model

ABSTRACT

The carbon emissions and cost during the construction phase are significant contributors to the oilfield lifecycle. As oilfields enter the late stage, the adaptability of facilities decreases. To achieve sustainable development, oilfield reconstruction was usually conducted in discrete rather than continuous space. Motivated by economic and sustainability goals, a 3-phase heuristic model for oilfield reconstruction was developed to mine potential locations in continuous space. In phase 1, considering the process characteristics of the oil and gas gathering system, potential locations were mined in continuous space. In phase 2, incorporating comprehensive reconstruction measures, a reconstruction model was established in discrete space. In phase 3, the topology was further adjusted in continuous space. Subsequently, the model was transformed into a single-objective mixed integer linear programming model using the augmented ε-constraint method. Numerical experiments revealed that the small number of potential locations could effectively reduce the reconstruction cost, and the quality of potential locations mined in phase 1 surpassed those generated in random or grid form. Case studies showed that cost and carbon emissions for a new block were reduced by up to 10.45% and 7.21 %, respectively. These reductions were because the potential locations mined in 1P reduced the number of metering stations, and 3P adjusted the locations of metering stations in continuous space to shorten the pipeline length. For an old oilfield, the load and connection ratios of the old metering station increased to 89.7% and 94.9%, respectively, enhancing operation efficiency. Meanwhile, recycling facilitated the diversification of reconstruction measures and yielded a profit of 582,573 ¥, constituting 5.56% of the total cost. This study adopted comprehensive reconstruction measures and tapped into potential reductions in cost and carbon emissions for oilfield reconstruction, offering valuable insights for future oilfield design and construction. © 2025 The Authors. Publishing services by Elsevier B.V. on behalf of KeAi Communications Co. Ltd. This is an open access article under the CC BY-NC-ND license (http://creativecommons.org/licenses/by-nc-nd/ 4.0/).

1. Introduction

As oilfields progress into the mid and late stages, the production of old wells continually declines, and the water cut rises to over 90% (Feng et al., 2022; Huang et al., 2023). Meanwhile, due to the uneven distribution of infrastructure and exploitation level in oilfield blocks, the oil and gas gathering system (OGGS) encounters inefficient operations in its late stage, such as the low load and high-cost operation at metering stations and pipelines (Ji et al., 2021; Bai et al., 2022). These inefficiencies can be alleviated by

* Corresponding author.

E-mail address: w.wang@cup.edu.cn (W. Wang).

reconstructing oilfields. Furthermore, the construction cost of the OGGS accounts for approximately 30%—40% of the total cost of oilfield construction (Rahmawati et al., 2012; Liu et al., 2015), and the carbon emissions during the construction phase are the highest among all sub-stages over the oilfield lifecycle (Huang et al., 2021; Xu et al., 2022). Thus, the old oilfield is taking a significant social responsibility for economic operation and environmental protection (Zhang et al., 2021; Wang et al., 2022; Tang and Li, 2023).

According to the production evolution law of oilfield, the lifecycle of an oilfield is divided into three phases: the rising production phase in the early stage, the stable production phase in the mid stage, and the decreasing production phase in the late stage (Silva and Guedes Soares, 2021; Sun et al., 2021; Ji et al., 2023).

However, several oilfields have entered the late stage of development and are facing a series of production challenges (Song et al., 2013; Yuan and Wang, 2018; Zhang et al., 2022). During this stage, the decline in formation energy leads to decreased production of old wells, reduced load ratio of station facilities, and excess capacity of gathering pipelines. The operation status of oilfields is not in the economic range (Yuan and Wang, 2018). Additionally, as the gathering radius of old wells gradually shortens, the current topology of the OGGS cannot ensure the safe and stable transportation of produced fluids to the processing facilities (He et al., 2019).

The problems mentioned above hinder the efficient operation of old oilfields, which can be mitigated through oilfield reconstruction. On the one hand, to ensure the sustainable development goal of increasing production in old oilfields, infill wells are drilled in old blocks to enhance oil recovery (Malallah et al., 2021), and new blocks are developed to increase production (Yan et al., 2021). Thus, it is vital to ensure that the new wells are compatible with existing facilities during reconstruction. On the other hand, in order to achieve economic and efficient operation of old blocks, some lowload metering stations and gathering pipelines may be recycled to improve the overall load ratio of the OGGS. However, integrating new wells into the existing system and recycling old facilities will change the topology and the operation status of the OGGS. Therefore, it is highly valuable to explore how to reconstruct oilfields in an economic and low-carbon manner to enhance the adaptability between the old and new blocks.

Previous work on the optimization of the oilfield surface system has primarily focused on new pipe networks. Zhou et al. (2015) decomposed the optimization of the new pipeline network into several sub-problems, including dividing well groups, locating metering stations, determining the connection of trunk lines, and optimizing pipe diameters. To make the design optimization model realistic, reservoir dynamics were modeled by Ramos Rosa et al. (2018), and the hydraulic characteristics of the gathering pipeline were considered by the piecewise linearization method (Hong et al., 2019). Additionally, Dbouk et al. (2021) introduced terrain undulations into the optimization model to project the optimization model in 3D space. Intelligent algorithms have also been employed to solve design optimization models (Wu et al., 2022; Yue et al., 2023; Liu et al., 2024). For example, unsupervised learning and clustering algorithms were used to divide well groups (Wang et al., 2021). Intelligent algorithms have the advantage of a fast solution but may fall into local optima as the model size increases (Liu et al., 2019, 2024). The above design optimizations of new pipeline networks, which consider new wells and ignore the impact of old systems, can no longer meet the needs of late-stage oilfield development.

There have been many studies on the reconstruction of various pipeline systems, especially water pipeline networks, but few on the OGGS. Due to the aging of pipes, some pipes were replaced, and Shin et al. (2016) developed an optimization model for rehabilitating water pipeline systems to minimize the costs of pipe replacement, renovation, and repair. The increase in precipitation reduced the adaptability of urban water drainage networks, so Iglesias-Rey et al. (2017) proposed a rehabilitation model whose decision variables included the rehabilitation and replacement of existing pipes, as well as the operation scheme of pumps. To address urban water supply disruptions caused by earthquakes, Taheri and Pishvaee (2024) developed a regret-based redesign optimization model for the urban water supply network to optimize water flow, construction locations, and pipeline connections. Although research on water pipeline system reconstruction provides a reference for old oilfields, there are obvious differences in their topologies and operation modes. Wang et al. (2018b)

established an optimization design model for restructuring the OGGS in the mid to late stages, which adopted measures for recycling pipelines and transfer stations but did not include constructing new pipelines. The above research focused on reconstruction optimization within the existing system. Natural gas transportation networks are often extended in the late stage, and multi-period construction optimization models have been established (Üster and Dilaveroğlu, 2014; Wang et al., 2018c; Hong et al., 2020). However, these models mainly decide on the new pipeline construction schemes at different periods, ignoring pipeline recycling. Overall, current optimization efforts on the OGGS reconstruction separate the internal reconstruction of existing systems from the integration of new systems, lacking comprehensive reconstruction measures that combine recycling with new construction of pipelines and facilities.

In the design of pipeline networks, station facilities, such as the metering station and transfer station, are co-located with wells in most studies, meaning that these optimization efforts are conducted in discrete space (Zhang et al., 2017; Wang et al., 2018a; Zhou et al., 2021). Few studies have focused on mining the potential locations of facilities in continuous space. Wang et al. (2012) and Silva and Guedes Soares (2019) assumed that the arithmetic mean of the coordinates of the wells in a well group was the optimal location of the metering station. He et al. (2019) assigned different production weights to wells, and took the sum of the product of the production weights and coordinates of wells as the construction location of the metering station. With the centroid position obtained through clustering representing the station location, Sánchez et al. (2022) applied the k-means clustering algorithm to address the recharging station location problem. The aforementioned methods are essentially weighting or clustering methods, and can not adjust the station facilities to the optimal location in continuous space. Moreover, the OGGS features special process characteristics, such as connection number and gathering radius constraints. The traditional Weiszfeld algorithm can address the station location problem in continuous space, but it does not apply to the gathering radius constraint (Weiszfeld and Plastria, 2008). Thus, considering the process constraints of the OGGS, little attention has been paid to obtaining high-quality potential locations for station facilities in continuous space.

The objective of network design optimization is usually investment cost (Ramos Rosa et al., 2018; Allen et al., 2022), reliability (He et al., 2019; Wu et al., 2022), and transported volume (Alves et al., 2016). However, the carbon footprints of the single pipeline, natural gas transmission system, and crude oil transmission were studied (Zubail et al., 2021; Xu et al., 2022; Chen et al., 2023), which found that the construction phase accounts for a significant portion of the total carbon emissions over the lifecycle. Hence, carbon emission assessment in the oilfield cannot be overlooked.

Concluded from the reviewed literature, although there are several optimization studies on the design of new pipeline networks, internal reconstruction of existing networks, and multiperiod network construction, oilfield reconstruction presents unique challenges. The reconstruction measures of oilfields are comprehensive, including the recycling of inefficient and high-cost facilities in the old system and the integration of the new system. Additionally, current pipeline design optimizations are often conducted in discrete space, leading to suboptimal facility locations. There exists a gap in mining high-quality potential locations of facilities in continuous space while accounting for the process characteristics of the OGGS. Lastly, it is necessary to consider the low-carbon in addition to the economy. To address the above limitations, this study developed a new design model for oilfield reconstruction to promote the sustainable development of oilfields,

which made the following contributions.

- (1) Taking various reconstruction measures, such as the recycling and new construction of pipelines and metering stations, a 3-phase heuristic model for the OGGS reconstruction was proposed. This model can provide economic and low-carbon construction schemes for the new block. Additionally, this model can connect new blocks and infill wells to the old oilfield, enhancing the adaptability between new and existing systems.
- (2) Considering the special process characteristics of the OGGS, phase 1 (1P) mined the potential locations of the newly-built metering station in continuous space. Phase 2 (2P) obtained the topology of the OGGS in discrete space. Phase 3 (3P) adjusted the locations of newly-built metering stations and the topology of OGGS in continuous space. These phases effectively mined the potential locations in continuous space.
- (3) With the economic and low-carbon goals, the optimization model could provide a reference for the decarbonization of the OGGS.
- (4) The superiority and applicability of the proposed model were demonstrated through numerical experiments and two case studies: one for a new block and another for an old oilfield.

2. Methodology

Fig. 1 shows the research framework of this study, consisting of data collection, the reconstruction optimization model for oilfields, numerical experiments, case studies, and results output modules.

2.1. Problem description

As an indispensable component of the oil and gas field surface system, the OGGS transports production fluid from wells to the central processing facility (CPF). The process flow of the OGGS is illustrated in Fig. 2(a). The production fluid from wells is metered at metering stations. Transfer stations are responsible for pressuring and heating the production fluid. The CPF dewaters natural gas, stabilizes crude oil, and recovers natural gas liquid. This study primarily focused on the scope from the well to the metering station, which incurs the highest construction cost and involves the most complex connection relationship among the entire process flow of the OGGS.

In the mid to late stages of oilfield development, the reduction in formation energy shortened the gathering radius of old wells. Moreover, some old facilities may deteriorate to a point where they are recycled because of the long-term operation. Therefore, the reconstruction measures shown in Fig. 2(b) were adopted to address these issues. If a metering station is recycled, the wells connected to it must be reassigned to other metering stations. Additionally, new wells in new blocks and infill wells in old blocks need to be integrated into the existing OGGS. In other words, as shown in Fig. 2(b), the pipelines were adjusted in following manners: one "reservation" (some pipelines connecting the old well and reserved metering station), three "recycling" (the pipelines connecting the abandoned well and reserved metering station, some pipelines connecting the old well and reserved metering station, and the pipelines connecting the old well to recycled metering station), and four "newly-built" (the pipelines connecting the old well and reserved metering station, old well to newly-built metering station, newly-built well to reserved metering station, and newly-built well to newly-built metering station).

To enhance solving efficiency, the following assumptions were made in this study.

- 1) There was no serial connection between the wells, and each well was connected to only one metering station.
- The scope from the well to the metering station was studied, while the scope from the metering station to the CPF was excluded.
- 3) The influences of pipeline height differences and obstacles were not considered.

2.2. Mathematical model

2.2.1. 1P: mining the potential locations of the newly-built metering station

The goal of 1P is to mine potential locations of the newly-built metering station outside the well sites, considering the process characteristics of the OGGS, such as the maximum processing capacity and connection number constraints of the metering station, as well as the gathering radius of the well. As shown in Fig. 3, circles are drawn with newly-built wells and old wells as the centers and the gathering radius of wells as the radius. The intersection points of these circles are defined as the set K^c .

In 1P, the candidate locations for the newly-built metering station consist of new wells, old wells, old metering stations, and intersection points, i.e., $K = I^n \cup I^o \cup J \cup K^c$. Where I^n is the set of new wells; I^o is the set of old wells; I is the set of old metering stations. Define I as the union of I^o , I^n , and I^c . Where I^c is the set of recycled wells. In addition, old metering stations and the pipelines connected to old wells were not recycled in 1P.

(1) Objective function

The objective of 1P is the minimum number of open metering stations, as follows:

$$\min F_1 = \sum_{k \in K} \nu_k \tag{1}$$

where, v_k is a 0-1 decision variable that determines the open scheme of the metering station in 1P, and if the metering station at point k is open, it equals 1; otherwise, it equals 0.

(2) Constraints

a) Facility existence constraints

If the recycling measure of old facilities is performed, some old metering stations will be recycled, and the mined potential locations may not adequately consider the topology information of the old system. Therefore, old metering stations are not recycled in 1P, as follows:

$$v_k = 1 \ \forall k \in J \tag{2}$$

In 1P, the pipeline-related reconstruction measures include constructing new pipelines and recycling the pipelines connecting to the abandoned wells, so the existence constraints of the pipeline are as follows:

$$B_{ikt} = Z_{ikt} - Z_{ikt}^{ab} + B_{ikt}^{n} \ \forall i \in I, \forall k \in J, \forall t \in T$$

$$(3)$$

where, B_{ikt} is a 0–1 decision variable, if a pipeline with specification t exists between well i and point k after optimization, it equals 1; otherwise, it equals 0. B_{ikt} determines the topology of the OGGS in 1P, including the connections between wells and metering stations as well as the pipeline specification. B_{ikt}^{n} is a 0-1 decision variable that determines the new construction scheme of the pipeline in 1P,

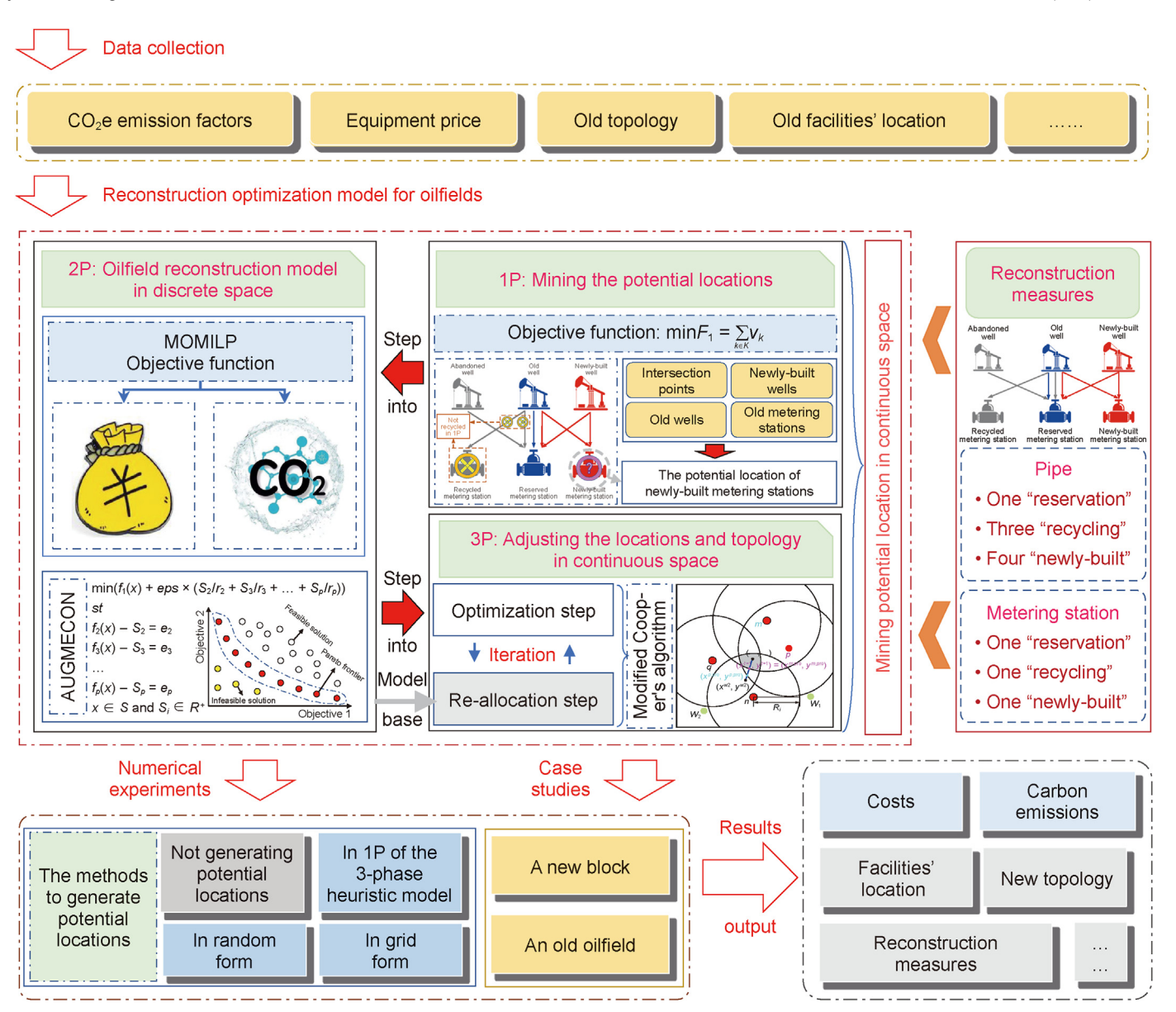
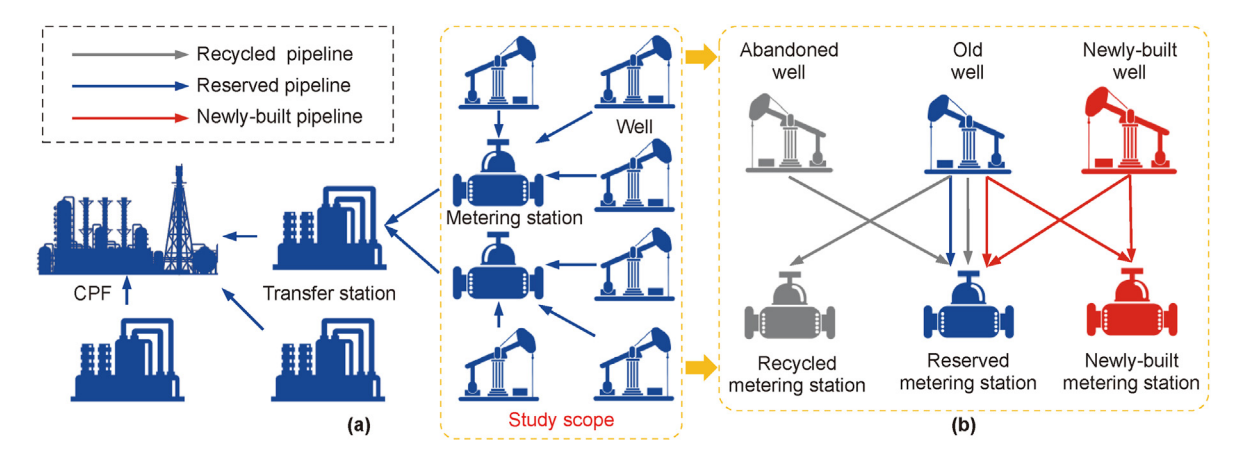


Fig. 1. Research framework of this paper.



 $\textbf{Fig. 2. (a)} \ \text{Process flow of the OGGS; (b)} \ \text{Reconstruction measures.}$

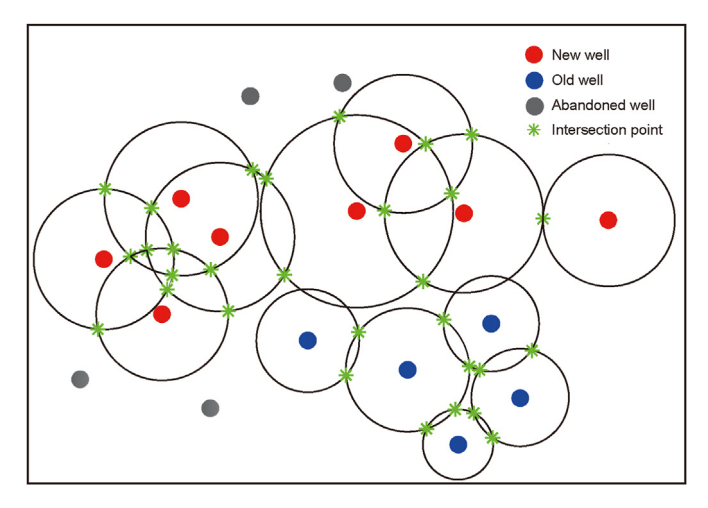


Fig. 3. Diagram of the intersection points of circles.

if a new pipeline with specification t is constructed between well i and point k, it equals 1; otherwise, it equals 0. Z_{ikt} is a known 0–1 variable that represents the topology of the existing system before 1P, if a pipeline with specification t exists between well t and point t before optimization, it equals 1; otherwise, it equals 0. t0. t1 variable that represents the connections between abandoned wells and old metering stations before 1P, if a pipeline with specification t1 exists between abandoned well t3 and point t4 before optimization, it equals 1; otherwise, it equals 0. t7 is the set of pipeline specifications.

b) Well constraints

The new and old wells are only connected to one metering station, while the abandoned well is not connected to the metering station because the pipelines connecting to the abandoned well will be recycled, as follows:

$$\sum_{k \in K} \sum_{t \in I} B_{ikt} = \mu_i^{\text{no}} \ \forall i \in I$$
 (4)

where, μ_i^{no} is a known 0–1 variable that represents the type of well, and if well i is a new well or an old well, it equals 1; if well i is an abandoned well, it equals 0.

Due to friction loss and heat loss, if the pipeline connecting the well and the metering station is too long, the fluid's temperature and pressure at the end of the pipeline become low, leading to potential accidents such as crude oil condensate and excessive back pressure (Liu et al., 2020). Therefore, the distance between a well and its connected metering station must be within the well's gathering radius, as follows:

$$\sum_{k=K} \sum_{t=T} B_{ikt} L_{ik} \le \sum_{k=K} \sum_{t=T} B_{ikt} R_{it} \ \forall i \in I$$
 (5)

where, L_{ik} is the distance between well i and point k. R_{it} is the gathering radius of the well i with specification t.

c) Old metering station constraints

The metering station has a fixed number of connection interfaces. Moreover, an excessive processing rate will overload the furnace and transfer pump in the metering station. Therefore, each old metering station must meet the requirements for connection

number and processing capacity, as follows:

$$\sum_{i \in I} \sum_{t \in T} B_{ikt} \le N_k^{\text{max}} \ \forall k \in J$$
 (6)

$$\sum_{i=I} \sum_{t=T} q_i B_{ikt} \le Q_k^{\text{max}} \ \forall k \in J$$
 (7)

where, q_i is the production rate of well i. N_k^{\max} is the maximum connection number of the old metering station at point $k \in J$. Q_k^{\max} is the maximum processing capacity of the old metering station at point $k \in J$.

d) Newly-built metering station constraints

Similarly to the old metering station, if a newly-built metering station is open at point $k \in K - J$, it must meet the requirements for the connection number and processing capacity, as follows:

$$\sum_{i \in I} \sum_{t \in T} B_{ikt} \le (1 - \nu_k) N + N^{\text{new,max}} \ \forall k \in K - J$$
 (8)

$$\sum_{i \in I} \sum_{t \in T} q_i B_{ikt} \le (1 - \nu_k) N + Q^{\text{new,max}} \ \forall k \in K - J$$
 (9)

where, $N^{\text{new,max}}$ is the maximum connection number of the newlybuilt metering station. $Q^{\text{new,max}}$ is the maximum processing capacity of the newly-built metering station. N is a sufficiently large number.

e) Economic flow velocity constraints

The flow velocity in the pipeline is a key factor in determining the appropriate pipeline specifications. To ensure the economic construction and operation of the gathering pipeline, the flow velocity should be within an economical range.

$$q_i \le \sum_{k \in K} \sum_{t \in T} B_{ikt} v^{\max} S_t \ \forall i \in I$$
 (10)

$$q_i \ge \sum_{k \in K} \sum_{t \in T} B_{ikt} v^{\min} S_t \ \forall i \in I$$
 (11)

where, v^{max} and v^{min} are the upper and lower bounds of the economic flow velocity, respectively. S_t is the cross-sectional area of the pipeline with specification t.

The model presented in 1P yields the decision variable v_k . If $v_k = 1$ $k \in K - J$, the point k becomes the potential location of the newlybuilt metering station. Define the set I^+ as the potential locations of the newly-built metering station.

2.2.2. 2P: oilfield reconstruction model in discrete space

The goal of 2P is to develop the oilfield reconstruction model in discrete space. The potential locations of the newly-built metering station mined by 1P contain extensive information about the process characteristics of the OGGS and thus serve as candidate locations for the newly-built metering station in 2P. These candidate locations for the newly-built metering station in 2P consist of new wells, old wells, old metering stations, and the potential locations of the newly-built metering station mined in 1P, i.e., $M = I^{\rm ID} \cup I^{\rm O} \cup I \cup I^{\rm T}$.

(1) Objective functions

a) Economic goal

The reconstruction cost includes the construction costs of newly-built metering stations and newly-built pipelines, as well as the recycling profits of old metering stations and old pipelines, as follows:

$$\min F_2^{\text{eco}} = C^{\text{SB}} + C^{\text{PB}} - C^{\text{SR}} - C^{\text{PR}}$$
 (12)

$$C^{\rm SB} = \sum_{m \in M} P_m^{\rm n} CB^{\rm s} \tag{13}$$

$$C^{\text{PB}} = \sum_{i=1} \sum_{m=M} \sum_{t=T} \left(L_{im} B_{imt}^{\text{n}} C B_t^{\text{p}} \right) \tag{14}$$

$$C^{SR} = \sum_{m \in I} P_m^c C R_m^s \tag{15}$$

$$C^{\text{PR}} = \sum_{i \in I} \sum_{m \in Ir} \sum_{t \in T} \left(L_{im} B_{imt}^{\text{c}} C R_t^{\text{p}} \right) \tag{16}$$

where, P_m^n is a 0–1 decision variable, and if a new metering station is constructed at point m, it equals 1; otherwise, it equals 0. P_m^c is a 0-1 decision variable, and if the old metering station at point m is recycled, it equals 1; otherwise, it equals 0. P_m^n , P_m^c determine the new construction and recycling schemes of the metering station in 2P, respectively. B_{imt}^{n} is a 0-1 decision variable, if a new pipeline with specification t is constructed between well i and point m, it equals 1; otherwise, it equals 0. B_{imt}^{c} is a 0–1 decision variable, and if the old pipeline with specification t between well i and point m is recycled, it equals 1; otherwise, it equals 0. B_{imt}^n , B_{imt}^c determine the new construction and recycling schemes of the pipeline in 2P, respectively, including the connections between wells and metering stations as well as the pipeline specification. C^{SB} , C^{PB} are the construction costs of newly-built metering stations and newly-built pipelines, respectively. CSR, CPR are recycling profits of old metering stations and old pipelines, respectively. CBs is the cost of constructing a new metering station. CR_m^s is the profit of recycling the old metering station at point m. CB_t^p is the cost of constructing the pipeline with specification t per unit length. CR_t^p is the profit of recycling the pipeline with specification t per unit length. L_{im} is the distance between well i and point m.

b) Environmental goal

The environmental objective is to minimize the total carbon emissions, including carbon emissions from the construction and recycling of metering stations and pipelines, as follows:

$$\min F_2^{\text{env}} = CE^{\text{SB}} + CE^{\text{PB}} + CE^{\text{SR}} + CE^{\text{PR}}$$
(17)

$$CE^{SB} = \sum_{m \in \mathcal{M}} P_m^n EB^s \tag{18}$$

$$CE^{PB} = \sum_{i=1} \sum_{m=Mt=T} \left(L_{im} B_{imt}^n EB_t^p \right) \tag{19}$$

$$CE^{SR} = \sum_{m \in M} P_m^c ER^s \tag{20}$$

$$CE^{PR} = \sum_{i=1} \sum_{m=1} \sum_{t=T} \left(L_{im} B_{imt}^{c} E R_{t}^{p} \right)$$

$$\tag{21}$$

where, CESB, CEPB are the carbon emissions of constructing newly-

built metering stations and newly-built pipelines, respectively. CE^{SR} , CE^{PR} are the carbon emissions of recycling old metering stations and old pipelines, respectively. EB^s , ER^s are the carbon emissions of constructing a new metering station and recycling an old metering station, respectively. EB_t^p is the carbon emissions of constructing the pipeline with specification t per unit length. ER_t^p is the carbon emissions of recycling the pipeline with specification t per unit length. EB^s , ER^s , EB^s , EB^t and ER^t are obtained by carbon footprint analysis (Chen et al., 2023), detailed in Supplementary Material, Section S3.

(2) Constraints

a) Facility existence constraints

The reconstruction measures for the metering station include reservation, recycling, and new construction, so the existence constraints of the metering station are as follows:

$$P_m^{\mathsf{s}} = P_m^{\mathsf{b}} + P_m^{\mathsf{n}} - P_m^{\mathsf{c}} \ \forall \, m \in M \tag{22}$$

$$P_m^{\mathsf{c}} \le P_m^{\mathsf{b}} \ \forall m \in M \tag{23}$$

where, $P_m^{\rm S}$ is a 0–1 decision variable that determines the reconstruction scheme of the metering station in 2P, and if a metering station exists at point m after reconstruction, it equals 1; otherwise, it equals 0. $P_m^{\rm b}$ is a known 0–1 variable that represents the existence scheme of the old metering station before reconstruction, and if a metering station exists at point m before reconstruction, it equals 1; otherwise, it equals 0. Eq. (22) determines whether there is a metering station at point m after reconstruction. Old metering stations may be recycled, as expressed in Eq. (23).

Similar to the metering station, the existence constraints of the pipeline are as follows:

$$B_{imt} = Z_{imt} - Z_{imt}^{ab} + B_{imt}^{n} - B_{imt}^{c} \quad \forall i \in I, \forall m \in M, \forall t \in T$$
 (24)

$$B_{imt}^{c} \leq Z_{imt} \ \forall i \in I, \forall m \in M, \forall t \in T$$
 (25)

where, B_{imt} is a 0–1 decision variable, and if there is a pipeline with specification t between well i and point m after reconstruction, it equals 1; otherwise, it equals 0. Z_{imt} is a known 0–1 variable, and if a pipeline with specification t exists between well i and point m before reconstruction, it equals 1; otherwise, it equals 0. Z_{imt}^{ab} is a known 0–1 variable, if a pipeline with specification t exists between abandoned well i and point m before reconstruction, it equals 1; otherwise, it equals 0. Eq. (24) determines whether there is a pipeline with specification t between well t and point t after reconstruction. Old pipelines may be recycled, as expressed in Eq. (25).

b) Well constraints

The new and old wells are only connected to one metering station, while the abandoned well is not connected to the metering station because the pipelines connected to the abandoned well will be recycled, as follows:

$$\sum_{m \in Mt \in T} \sum_{i=1}^{no} B_{imt} = \mu_i^{\text{no}} \ \forall i \in I$$
 (26)

The new and old wells must meet the gathering radius constraint, as follows:

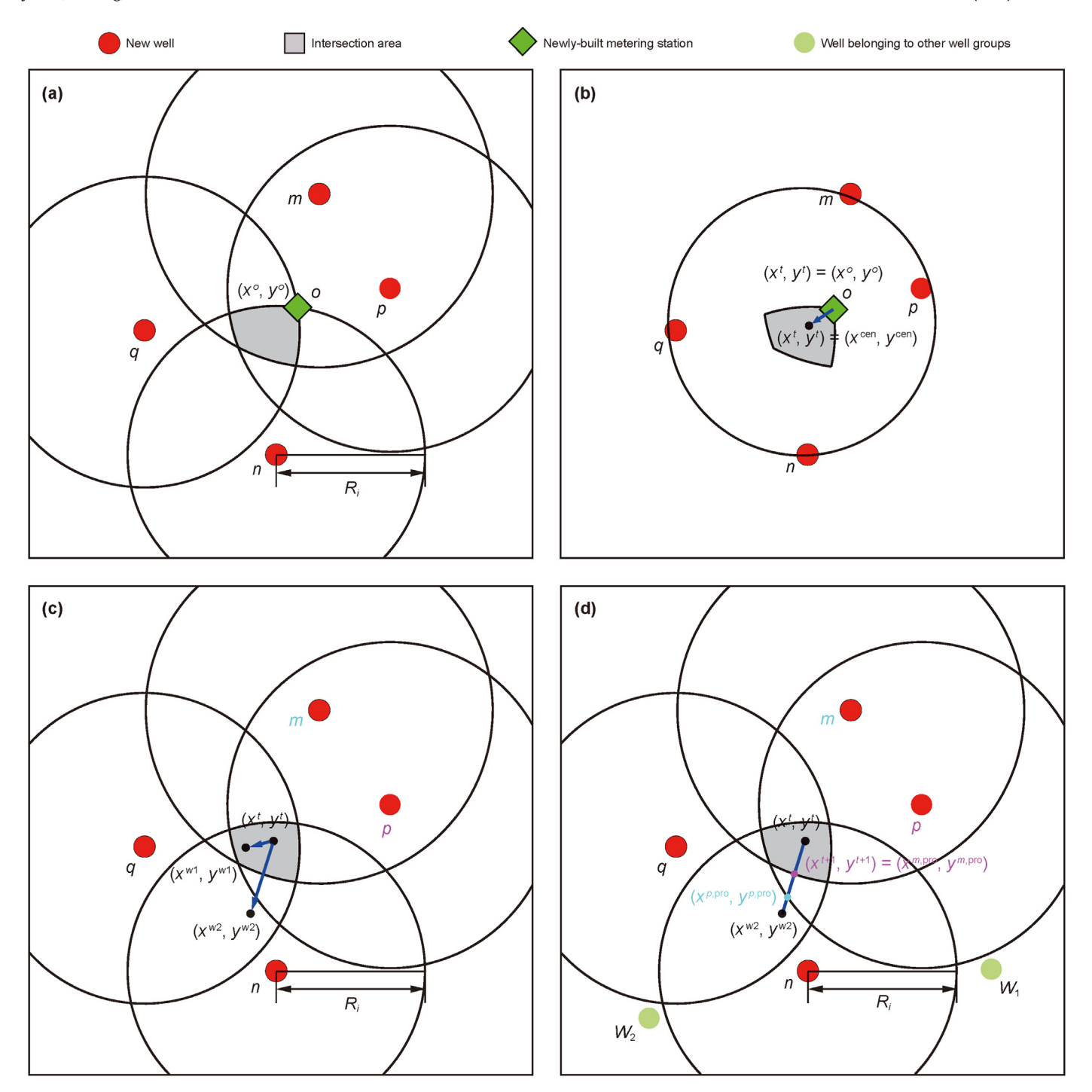


Fig. 4. The optimization step in continuous space.

$$\sum_{m \in Mt \in T} B_{imt} L_{im} \leq \sum_{m \in Mt \in T} B_{imt} R_{it} \ \forall i \in I$$
 (27)
$$\sum_{i \in I} \sum_{t \in T} B_{imt} \leq \left(1 - P_m^b + P_m^c\right) N + N_m^{max} \ \forall m \in J$$
 (28)

c) Old metering station constraints

If there is an old metering station at point *m* after reconstruction, this station must satisfy the requirements for the connection number and processing capacity, as follows:

$$\sum_{i \in I} \sum_{t \in T} q_i B_{imt} \le \left(1 - P_m^b + P_m^c\right) N + Q_m^{\text{max}} \ \forall m \in J$$
 (29)

where, N_m^{\max} is the maximum connection number of the old metering station at point $m \in J$. Q_m^{\max} is the maximum processing capacity of the old metering station at point $m \in J$.

d) Newly-built metering station constraints

Similarly to the old metering station, newly-built metering stations must satisfy the requirements for connection number and processing capacity, as follows:

$$\sum_{i=1}^{N} \sum_{t=1}^{N} B_{imt} \le (1 - P_m^n) N + N^{\text{new,max}} \forall m \in M$$
(30)

$$\sum_{i=1}\sum_{t=T}q_{i}B_{imt} \leq (1-P_{m}^{n})N + Q^{\text{new,max}} \ \forall m \in M$$
 (31)

e) Economic flow rate constraints

$$q_i \le \sum_{m \in M} \sum_{t \in I} B_{imt} v^{\max} S_t \ \forall i \in I$$
 (32)

$$q_i \ge \sum_{m \in Mt \in T} B_{imt} v^{\min} S_t \ \forall i \in I$$
 (33)

The model presented in 2P can provide a reconstruction solution in discrete space, which includes the construction locations of newly-built metering stations and new pipelines, and whether old metering stations and old pipelines should be recycled.

2.2.3. 3P: adjusting the locations of metering stations and topology in continuous space

The reconstruction scheme provided by 2P is optimal only in discrete space. However, the newly-built metering station could be located anywhere in the continuous space that satisfies the gathering radius constraint for each well in the well group. Thus, there is a possibility for improvement in the locations of newly-built metering stations and the connection relationships between wells and metering stations. To address this issue, Cooper's algorithm, which consists of an optimization step in continuous space and a re-allocation step in discrete space, is employed (Cooper, 1964). The optimization step optimizes the locations of metering stations in continuous space, followed by the re-allocation step to adjust the connection relationships. These steps alternate until the topology cannot be further improved. The traditional Weiszfeld algorithm is commonly used to solve the optimization step, but it has a limitation as it cannot consider the gathering radius constraint (Vardi and Zhang, 2001). Therefore, a projection operation was incorporated into the Weiszfeld algorithm in the optimization step to consider the gathering radius constraint, and the modified Cooper's algorithm is as follows.

Step 1 (S1): The optimization step in continuous space

Fig. 4 illustrates the procedure for S1 with an example. As shown in Fig. 4(a), four new wells are connected to one newly-built metering station. The gathering radius of each well was expressed as:

$$R_i = \sum_{m \in Mt \in T} B_{imt} R_{it} \ \forall i \in I$$
 (34)

Define well group set $C = \{p, q, m, n\}$. Point O is the location recommended by 2P for a newly-built metering station. S1 adjusts the point O to the optimal location within the intersection area in Fig. 4(a). The projection operation incorporated into the Weiszfeld algorithm is described in detail below:

(1) As shown in Fig. 4(b), $(x^{\text{cen}}, y^{\text{cen}})$ is the center of the smallest circle that encloses all wells in the set C. If $(x^{\text{cen}}, y^{\text{cen}})$ lies in

- the intersection area, then define the initial iteration location $(x^t, y^t) = (x^{\text{cen}}, y^{\text{cen}});$ otherwise, $(x^t, y^t) = (x^o, y^o).$
- (2) Get the recommended location (x^w, y^w) by the traditional Weiszfeld algorithm (Vardi and Zhang, 2001). As shown in Fig. 4(c), if (x^w, y^w) lies in the intersection area, i.e., $(x^w, y^w) = (x^{w1}, y^{w1})$, set the next iteration location $(x^{t+1}, y^{t+1}) = (x^{w1}, y^{w1})$, and proceed to step (4); if (x^w, y^w) does not lie in the intersection area, i.e., $(x^w, y^w) = (x^{w2}, y^{w2})$, and go to step (3).
- (3) The detailed procedure for step (3) is as follows:
- ① Define set $S \subset C$ as the wells that do not satisfy the gathering radius constraint relative to (x^w, y^w) . As shown in Fig. 4(c), $S = \{m, p\}$.
- ② Define (x^s, y^s) as the coordinate of a well s ∈ S. Define set B as the points that are R_s away from well s and lie on the segment connecting (x^t, y^t) and (x^w, y^w) . As shown in Fig. 4(d), $B = \{(x^{p,\text{pro}}, y^{p,\text{pro}}), (x^{m,\text{pro}}, y^{m,\text{pro}})\}$. The point in the set B that is cloest to (x^t, y^t) is chosen as the next iteration location (x^{t+1}, y^{t+1}) , i.e., $(x^{t+1}, y^{t+1}) = (x^{m,\text{pro}}, y^{m,\text{pro}})$.

The derivation of the mathematical expression of step (3) is detailed in Supplementary Material, Section S1.

(4) If $|(x^{t+1}, y^{t+1}), (x^t, y^t)| \le \varepsilon_1$, go to (S2), otherwise, return to step (2). ε_1 is a small value.

Step 2 (S2): The re-allocation step in discrete space

As shown in Fig. 4(d), the recommended location of the newly-built metering station is moved from (x^t, y^t) to (x^{t+1}, y^{t+1}) . If there are W_1 and W_2 wells near the well group set C, the distances between the recommended location and both W_1 and W_2 wells become shorter, and it is possible that W_1 and W_2 wells may be merged into the well group set C from other well groups. The connection between wells and metering stations can be further optimized by modifying the optimization model of 2P.

The modification to the model of 2P is that the locations of newly-built metering stations are predetermined by S1, so only the connection relationship between the metering station and the well is optimized in S2. For example, the location of a newly-built metering station is moved from point O to (x^m, y^m) as shown in Fig. 4(d), and then the location of this newly-built metering is predetermined as (x^m, y^m) in the model of 2P.

If the change in the objective goal does not meet the accuracy requirement ($\Delta F_2 \leq \varepsilon_2$), return to S1; otherwise, the loop ends. ε_2 is a small value.

2.3. Solving methods

There was a clear trade-off between economic and environmental goals, and the augmented ε-constraint method (AUGME-CON) was adopted to solve the multi-objective model in 2P (Mavrotas, 2009; Mavrotas and Florios, 2013). Further details about the AUGMECON are presented in Supplementary Material, Section S2. Besides, the optimization models of 1P and 2P, and the reallocation step in 3P are mixed integer linear programming (MILP) models, which were solved by the optimization solver GUROBI 11.0 based on the branch and bound algorithm (Neumann et al., 2022). As an algorithm for solving the MILP model, the branch and bound algorithm is known for high stability and the ability to find the globally optimal solution (Tomazella and Nagano, 2020). Its basic principle involves initially relaxing integer variables into continuous variables to convert the original problem into a relaxed problem. Subsequently, the feasible solution space is continually

23.94 9.83 5.34 optimization ratio of cost, % 21.71 17.28 8.25 24.16 12.81 6.62 8.77 5.21 newly-built metering stations $(Num_{\rm cp}^{3P})$ The number of 21.9 13.7 10.3 41.3 25.9 62.5 53.8 65.8 40.1 19.1 $-C_{cp}^{3p}$) $/C_{wp}^{3p} \times 100\%$, δ^{2p} and δ^{3p} characterized the optimization effect of the potential locations mined in 1P of 2P and 3P, respectively. Cost (C^{3P}₂), 10³ **136,803** 108,529 101,459 24,978 19,110 17,246 47,890 36,904 32,848 80,472 62,658 57,390 3Р Computation Cost Computation (C_{cp}^{2P}) , 10^3 time (t_{cp}^{2P}) , s **20.4** 19.6 38.3 4. 2. 2. 5.1 4.9 4.8 0.3 **139,593** 110,604 102,554 37,910 33,620 82,080 64,067 58,260 25,618 19,662 17,584 49,011 The number of left in $2P (add^2)$ the potential With potential location (considering 1P) 36.1 23.2 9.0 **60.8** 38.0 7.9 Computation time $(t_{\rm CD}^{\rm 1P})$, s 1.4 2.7 4.5 6.9 23.9 02.5 396.7 1159.2 The number of potential locations (add^{1p}) 14.1 10.2 8.1 28.0 20.6 16.1 **82.6** 56.2 43.1 newly-built metering stations (Num_{wp}^{3P}) The number of Without potential location (without considering 1P) **162.4** 86.9 57.4 31.4 20.5 13.9 59.5 39.3 25.6 100.9 58.0 $(C_{\rm wp}^{3p}), 10^3$ 1**79,860** 120,358 107,183 108,139 73,150 61,823 32,728 23,707 19,443 62,552 45,711 36,429 Cost Computation $10^3 \text{ time } (t_{wp}^{2P}), \text{ s}$ $= (C_{wp}^{3P} -$ 1.1 **17.0** 17.4 19.7 0.3 4.1 4.2 **180,152** 121,233 108,191 $-\left.C_{cp}^{2P}\right)/C_{wp}^{2P}\times100\text{\%, }\delta^{3P}$ 108,234 $(C_{\rm wp}^{\rm 2P}), 1$ 73,478 62,390 32,741 23,759 62,602 45,827 36,643 19,564 Cost No. The number Gathering of wells radius, m 1000 1000 1000 1500 $= (C_{wD}^{2P} \cdot$ (10) 400 100 200 Note: δ^{2P} 686 (5)

Optimization effect of the 1P and 3P.

partitioned into subregions (branch), and the lower bound for each branch is computed (bound). Ultimately, the optimal solution is found through iterative cycles (Watanabe et al., 2023; Denat et al., 2024).

3. Numerical experiments

The numerical experiments aimed to verify the optimization effect of the potential locations of the newly-built metering station mined in 1P and the modified Cooper's algorithm in 3P. The following cases were compared: (1) potential locations were not generated, i.e., the 3-phase heuristic model without considering 1P; (2) potential locations were mined in 1P of the 3-phase heuristic model, i.e., the 3-phase heuristic model considering 1P.

In numerical experiments, the locations of wells were generated randomly. The number of wells was [50, 100, 200, 400], and the gathering radius was [1000, 1,500, 2,000, 2500] m, respectively. The production rate of a new well is 150 m³/d. The basic parameters for the pipeline and metering station are detailed in Supplementary Material, Section S3, and a detailed description of the symbols used in the numerical experiments is shown in Supplementary Material, Section S4. To minimize random error, each numerical experiment was repeated 20 times, and the averaged results are shown in Table 1. The computation time of 3P was less than 1 s, so it was not reported in Table 1. The mathematical models were run on a personal computer with 16 GB RAM, an AMD Ryzen 3700X 8-Core Processor (3.6 GHz) and a Radeon RX 590 Series graphics card.

As shown in Table 1, the potential locations of the newly-built metering station mined in 1P significantly cut the costs. For example, in numerical experiment No. (10), 82.6 potential locations of the newly-built metering station were added, and the cost in 2P fell from 1.802 \times 10⁸ to 1.396 \times 10⁸ ¥, leading to an optimization ratio of 22.51%. Meanwhile, the cost in 3P fell from 1.799×10^8 to 1.368×10^8 ¥, with an optimization ratio of 23.94%. Moreover, it was observed that the number of newly-built metering stations considering 1P (Num_{cn}^{3P}) was overall much smaller than the number of metering stations without considering 1P (Num_{WD}^{3P}) . The above phenomenon inferred that the reason for the cost reduction is that the potential locations mined in 1P can significantly decrease the number of newly-built metering stations. As for the computation time of 2P, because of the small number of potential locations mined in 1P, there was no significant difference in the computation of 2P time between the

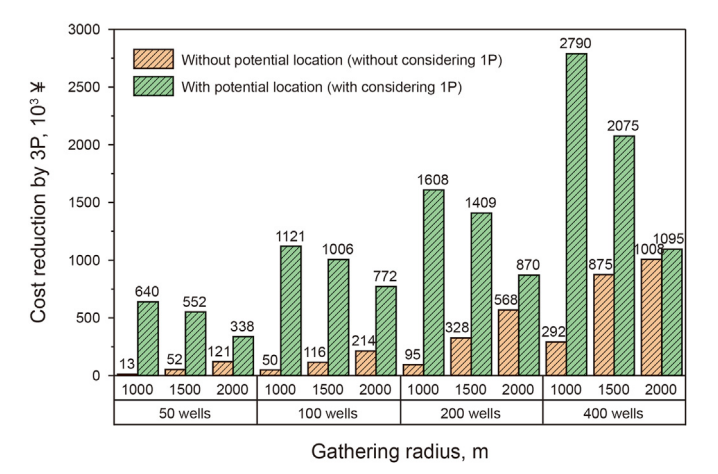


Fig. 5. Cost reductions after applying 3P.

Petroleum Science 22 (2025) 035_055

Table 2Comparison of different methods for generating potential locations.

No.	The number of wells	Gathering radius,m			2P			3P				The selection	
					The cost of 2P, 10 ³ ¥		The optimization ratio of 2P, %	The cost of 3P, 10 ³ ¥		The optimization ratio of 3P, %	ratio of potential locations, %		
			Random form (add ^{rg})	1P of the 3- phase heuristic model (add ^{1P})	Random form (C_{ran}^{2P})	Grid form ($C_{ m gri}^{ m 2P}$)	1P of the 3- phase heuristic model (C_{cp}^{2P})	C	Random form (C_{ran}^{3P})	Grid form ($C_{ m gri}^{ m 3P}$)	1P of the 3- phase heuristic model (C_{cp}^{3P})	Ü	$\eta_{ m ran}$ $\eta_{ m gri}$ $\eta_{ m cp}$
(1) (2) (3)	50	1000 1500 2000	33.4 23.5 19.6	14.1 10.2 8.1	31,923 22,933 18,492	31,650 22,942 18,537	25,618 19,662 17,584	19.75 19.06 14.27 14.30 4.91 5.14	31,886 22,795 18,319	31,600 22,788 18,341	24,978 19,110 17,246	21.66 20.96 16.16 16.14 5.85 5.97	8.05 8.13 80.14 7.85 7.93 74.38 6.87 6.25 55.28
(4) (5) (6)	100	1000 1500 2000	63.3 47.7 36.0	28.0 20.6 16.1	60,741 44,347 35,425	60,640 44,254 35,453	49,011 37,910 33,620	19.31 19.18 14.51 14.33 5.10 5.17	60,657 44,113 35,047	60,535 43,995 35,123	47,890 36,904 32,848	21.05 20.89 16.34 16.12 6.27 6.48	7.98 7.81 78.00 7.28 7.77 72.33 6.70 5.14 51.71
(7) (8) (9)	200	1000 1500 2000	106.5 75.9 58.8	48.2 33.9 25.0	103,338 71,645 59,544	102,909 71,641 59,379	82,080 64,067 58,260	20.57 20.24 10.58 10.57 2.16 1.88	103,066 71,115 58,905	102,624 71,048 58,740	80,472 62,658 57,390	21.92 21.59 11.89 11.81 2.57 2.30	7.04 7.27 74.87 6.49 6.95 68.44 4.81 4.32 35.87
(10) (11) (12)		1000 1500 2000	177.1 122.2 97.2	82.6 56.2 43.1	173,248 118,987 103,534	172,520 119,014 103,524	139,593 110,604 102,554	19.43 19.09 7.05 7.07 0.95 0.94	172,660 117,817 102,522	171,890 117,832 102,577	136,803 108,529 101,459	20.77 20.41 7.88 7.90 1.04 1.09	6.69 7.05 73.61 6.36 6.14 67.53 3.60 3.66 18.35

Note: ① $\lambda_{\text{ran}}^{2P} = (C_{\text{ran}}^{2P} - C_{\text{cp}}^{2P})/C_{\text{ran}}^{2P} \times 100\%$, $\lambda_{\text{gri}}^{2P} = (C_{\text{gri}}^{2P} - C_{\text{cp}}^{2P})/C_{\text{gri}}^{2P} \times 100\%$, $\lambda_{\text{ran}}^{3P} = (C_{\text{ran}}^{3P} - C_{\text{cp}}^{3P})/C_{\text{ran}}^{2P} \times 100\%$, $\lambda_{\text{gri}}^{3P} = (C_{\text{gri}}^{3P} - C_{\text{cp}}^{3P})/C_{\text{gri}}^{2P} \times 100\%$. ② η_{ran} , η_{gri} and η_{cp} are the selection ratio of potential locations. The selection ratio of potential locations = The number of potential locations left in 2P from the set I^+ ÷ The number of the potential locations of the newly-built

② η_{ran} , η_{gri} and η_{cp} are the selection ratio of potential locations. The selection ratio of potential locations = The number of potential locations left in 2P from the set I^+ ÷ The number of the potential locations of the newly-built metering station (add^{rg} or add^{1P}) × 100%.

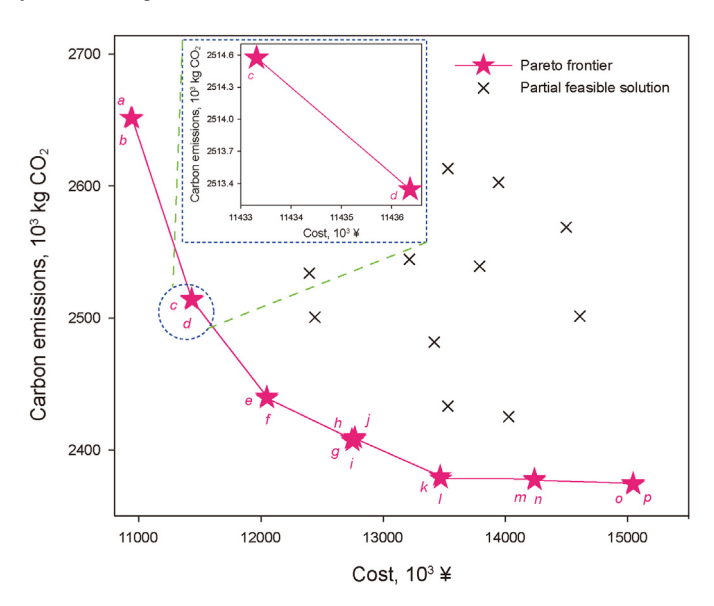


Fig. 6. Pareto frontier of case 1.

numerical experiment that mined potential locations in 1P ($t_{\rm cp}^{\rm 2P}$) and not generating potential locations ($t_{\rm wp}^{\rm 2P}$). In numerical experiment No. (10), 82.6 potential locations increased the calculation time of 2P from 17.0 to 20.4 s.

The modified Cooper's algorithm in 3P could lower the pipeline construction cost, thus reducing the total cost. Fig. 5 shows the cost reductions after applying 3P when potential locations of the newlybuilt metering station were mined in 1P, as well as when the potential location of the newly-built metering stations was not generated. In 3P, the connection relationship between metering stations and wells was adjusted, while the number of newly-built metering stations remained unchanged. Consequently, the cost reductions after applying 3P quantified the reduction in pipeline construction cost. Furthermore, the cost reductions after applying 3P with potential locations were larger than those without potential locations. For example, in numerical experiment No. (10), when the potential locations mined in 1P, the cost reduction was $2.79 \times 10^6 \, \text{W}$ which was larger than the cost reduction ($2.92 \times 10^5 \, \text{W}$) when there were no potential locations. Thus, it was found that the potential locations mined in 1P had an indirect optimization effect on the cost of 3P. Finally, as the gathering radius increased, the gap between the cost reductions after applying 3P with potential locations and those without potential locations was gradually narrowed.

To evaluate the quality of the potential locations mined in 1P, three methods for generating potential locations were compared: (1) potential locations mined in 1P of the 3-phase heuristic model, (2) potential locations generated in random form, and (3) potential locations generated in uniform (grid) form. To further demonstrate the superiority of method (1), if method (1) generated n potential locations, methods (2) and (3) generated $(\text{ceil}(\sqrt{2n}))^2 \geq 2n$ potential locations.

The potential locations of the newly-built metering station mined in 1P exhibited high quality. As indicated in Table 2, for 2P, the costs obtained by method (2) ($C_{\rm ran}^{\rm 2P}$) and method (3) ($C_{\rm gri}^{\rm 2P}$) were higher than those obtained by method (1) ($C_{\rm cp}^{\rm 2P}$). For example, in numerical experiment No. (10), the optimization ratios of 2P in random ($\lambda_{\rm ran}^{\rm 2P}$) and grid ($\lambda_{\rm gri}^{\rm 2P}$) forms were 19.43% and 19.09%, respectively. The previous law also held for 3P, as evidenced by the

fact that the costs obtained by method (2) ($C_{\rm ran}^{3P}$) and method (3) ($C_{\rm gri}^{3P}$) were higher than those obtained by method (1) ($C_{\rm cp}^{3P}$). For example, in numerical experiment No. (10), the optimization ratios of 3P in random ($\lambda_{\rm ran}^{3P}$) and grid ($\lambda_{\rm gri}^{3P}$) forms were 20.77% and 20.41%, respectively. Furthermore, the selection ratios of potential locations generated by methods (2) ($\eta_{\rm ran}$) and (3) ($\eta_{\rm gri}$) were lower than those by method (1) ($\eta_{\rm cp}$). Overall, despite the higher numbers of potential locations generated by method (2) and method (3) compared to method (1), the optimization effects achieved by method (2) and method (3) were lower than those achieved by method (1).

4. Case studies

Two hypothetical cases were selected as research objects to validate the superiority and applicability of the proposed model in both new block construction and old oilfield reconstruction.

4.1. Case 1: A new block

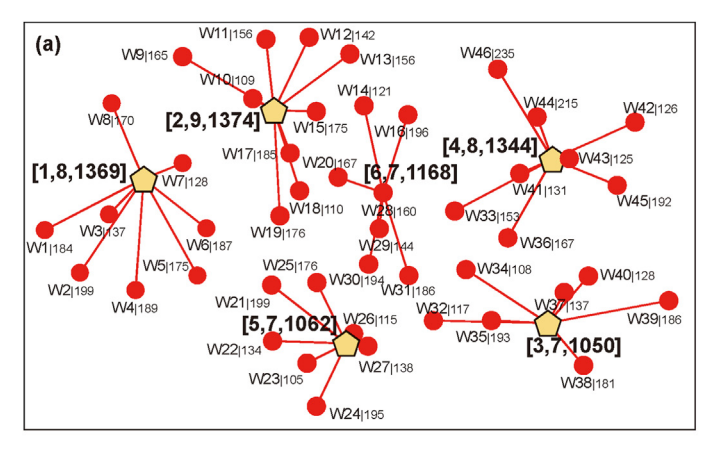
In this case, the basic data for 46 new wells are presented in Fig. 7(a). The notation "a|b" next to the new well represents "well number| production rate". The notation [i, j, k] next to the metering station represents [metering station number, number of wells connected to the metering station, amount of fluid processed at the metering station].

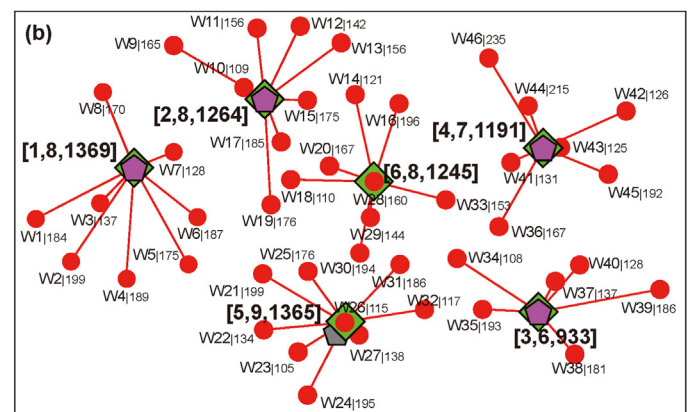
As shown in Fig. 6, there are 16 Pareto frontier points, each representing an optimal solution. Some of the Pareto frontier points are close to each other, and enlarged views of points c and d are given at the top of Fig. 6. Point a (economic goal) and point p (environmental goal) were selected for further analysis.

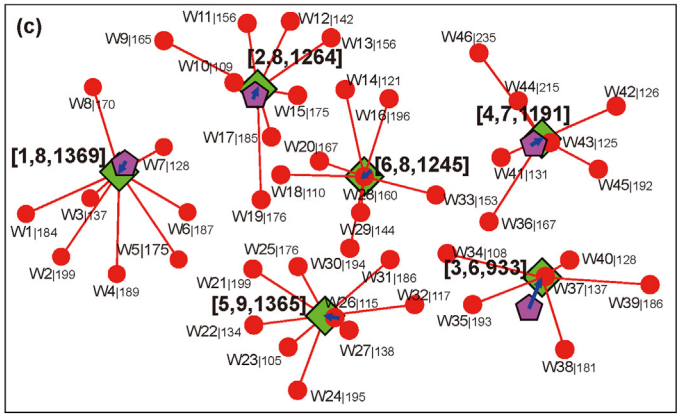
The optimization process under the economic goal is shown in Fig. 7. Fig. 7(a) presents the optimal solution for 1P, involving five potential locations for newly-built metering stations. The optimal solution for 2P is shown in Fig. 7(b), where the metering stations [1], [2], [3], and [4] were from potential locations, resulting in the selection ratio of potential locations being 80%. However, the potential location where metering station [5] was located in Fig. 7(a) was abandoned, and metering station [5] was constructed at W26 in Fig. 7(b).

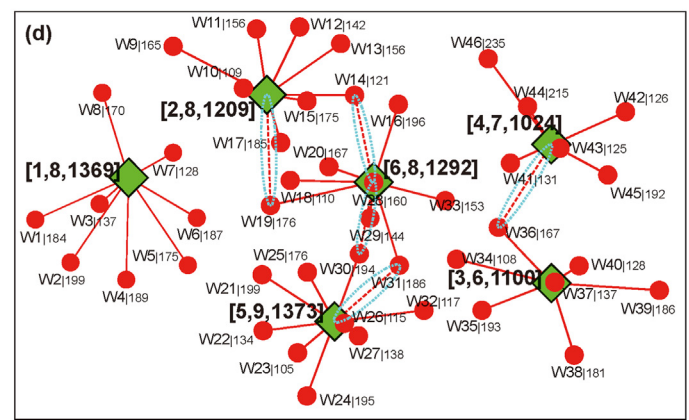
The 3P was iterated three times. Fig. 7(c) and (d) shows the first iteration. Fig. 7(c) illustrates the optimization process of S1, where the locations of all six metering stations changed, with metering station [3] undergoing the most significant adjustment. Furthermore, Fig. 7(d) illustrates the optimization process of S2. As the distance between metering station [3] and W36 was shortened in S1, W36 was assigned to metering station [3] from metering station [4] in S2. Similarly, the connection relationships of W14, W19, W30, and W31 also changed due to the location changes of metering stations in S1.

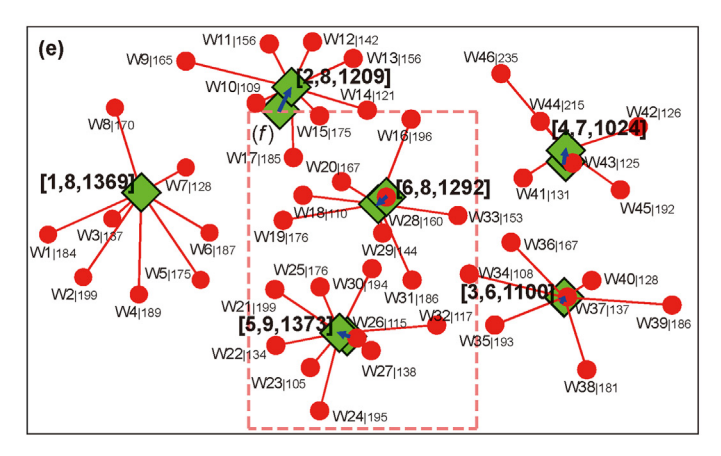
Fig. 7(e) and (f_1) shows the second iteration. Fig. 7(e) shows the optimization process of S1, and the locations of metering stations whose connections changed in the first iteration were adjusted. Taking the metering station [6] as an example, it no longer connected to W14 on its up and W30 on its below, while the W19 on its left was merged into it from the metering station [2], as shown in Fig. 7(d). Consequently, as shown in Fig. 7(e), the metering station [6] moved in the direction closer to W19 to reduce the pipeline length. The optimization process of S2 is shown in Fig. 7(f₁), where W31 and W30 were reconnected to metering stations [5] and [6], respectively. Fig. 7(f₂) shows the third iteration. The locations of the metering stations [5] and [6] changed slightly, while the topology of the OGGS did not change. The final topology and pipeline

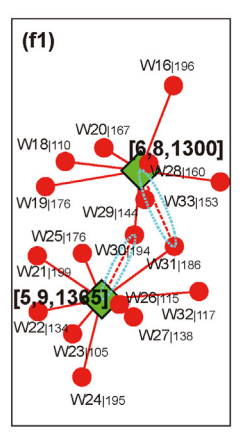












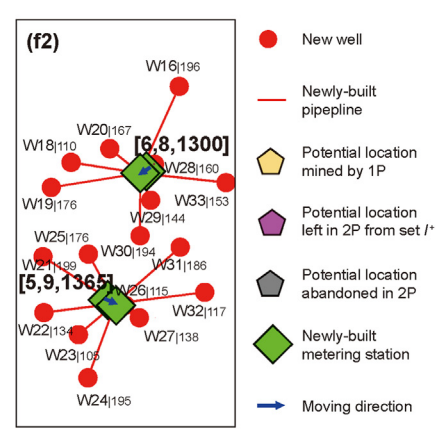


Fig. 7. The optimization processes of (a) 1P, (b) 2P, and (c-f) 3P under the economic goal.

specifications are shown in Fig. 1 and Table S6, Section S5.1.

In previous pipeline network design optimizations, metering stations were typically co-located with wells, meaning the optimization studies were conducted in discrete space. Thus, the optimization result of 2P without generating potential location was employed as the baseline case in this study. Compared to the baseline case, the proposed model had significant advantages. Table 3 presents the optimal results with different methods. In the baseline case, the cost and carbon emissions were 12,314,257 ¥ and 2,558,301 kg CO₂e, respectively. Under the economic goal, the 1P of the proposed model mined five potential locations, and four of them remained in 2P, resulting in a high selection ratio of 80%. Compared to the baseline case, the cost in 2P decreased to 11,187,881 ¥, achieving an optimization ratio of 9.15%. The cost in 3P

decreased to 2,651,562 ¥, with an optimization ratio of 10.45%. Under the environmentally optimal conditions, the total carbon emissions were reduced to 2,373,840 kg CO₂e, which was 7.21% lower than those of the baseline case (2,558,301 kg CO₂e).

Furthermore, the 3P of the proposed model effectively reduced the cost and carbon emissions, and the potential locations mined in 1P could enhance the optimization effect of 3P. Building on the baseline case, adjusting the locations of metering stations in continuous space through 3P decreased the cost from 12,314,257 to 12,212,186 \pm , achieving an optimization ratio of 0.83%. Meanwhile, the carbon emissions were decreased from 2,558,301 to 2,520,365 kg CO₂e, achieving an optimization ratio of 1.48%. However, when potential locations were mined in 1P of the proposed model, the 3P reduced the cost from 11,187,881 to 10,935,888

Table 3Optimal results with different methods.

		Without generating potential location (no 1P)	Economic g	oal	Environmental goal		
			Generating potential location			In 1P	
			In 1P	In the random	In the grid		
1P	Number of intersection points Number of newly-built metering stations Number of potential locations mined in 1P	 	970 6 5	/ / 16	/ / 16	970 12 5	
2P	Length of the newly-built pipe, m Cost, ¥ Carbon emissions, kg CO ₂ e	31,672 12,314,257 2,558,301	38,086 11,187,881 2,757,023	35,779 11,873,690 2,711,208	31,626 12,307,967 2,559,322	37,262 15,075,656 2,388,309	
3P	Number of newly-built metering stations Length of the newly-built pipe, m Cost, \pm Carbon emissions, kg $\mathrm{CO}_2\mathrm{e}$	8 30,923 12,212,186 2,520,365	6 36,236 10,935,888 2,651,562	7 34,519 11,702,009 2,636,863	8 30,824 12,198,758 2,511,892	10 37,057 15,047,776 2,373,840	
Cos	st optimization ratio of 2P (vs. no 1P), % st optimization ratio of 3P (vs. no 1P), % st optimization ratio of 3P (vs. 2P), %	0.83	9.15 10.45 2.25	3.58 4.18 1.45	0.05 0.11 0.89	-34.75 (vs. economic goal) -37.60 (vs. economic goal) 0.18	

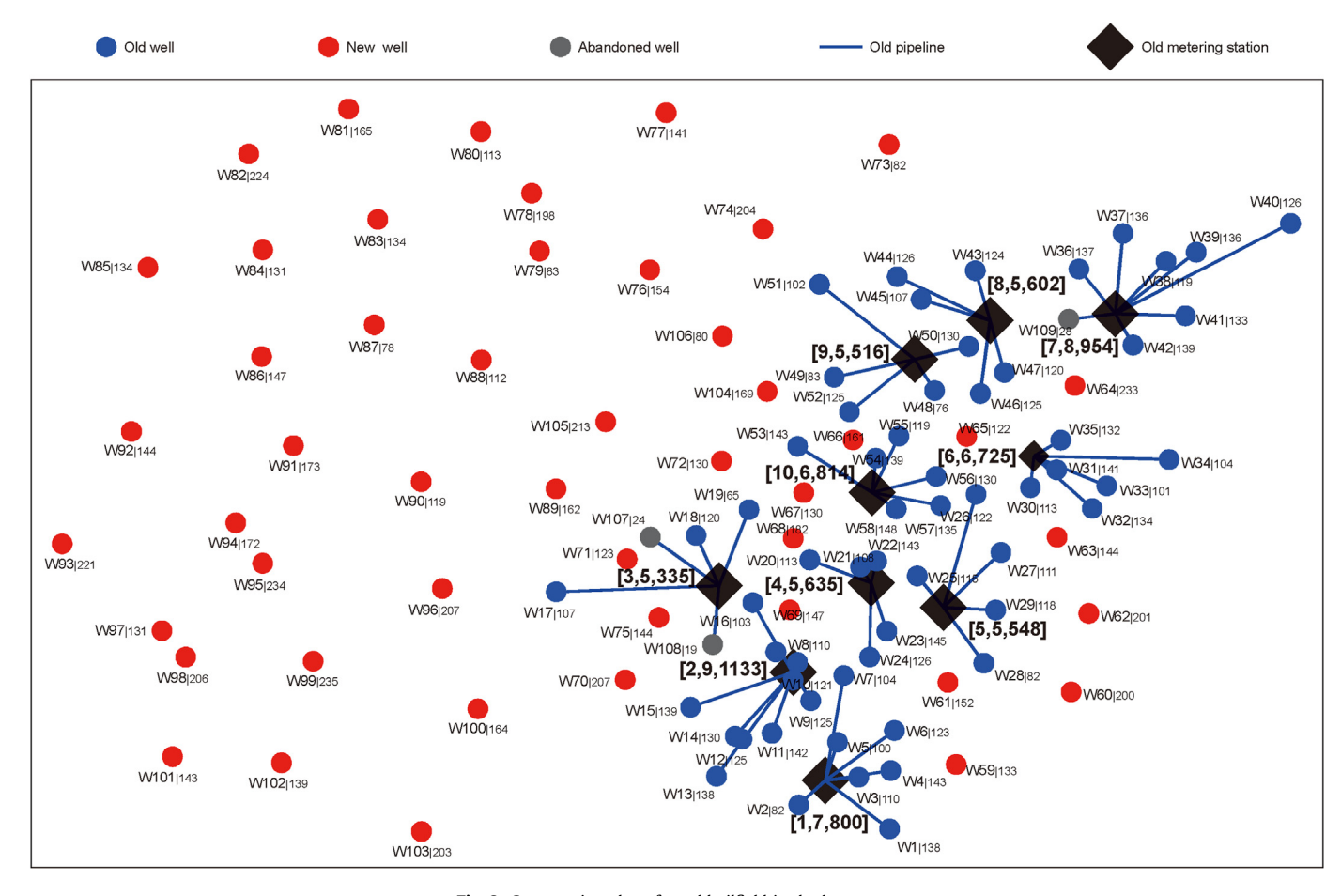


Fig. 8. Construction plan of an old oilfield in the late stage.

¥, with the cost optimization ratio increasing to 2.25%. Meanwhile, the carbon emissions decreased from 2,757,023 to 2,651,562 kg CO₂e, with the carbon emission optimization rate rising to 3.8%. The reason why 3P could reduce carbon emissions and cost lies in the shortened length of newly-built pipelines. Since 2P took the new wells, old wells, old metering stations, and the potential locations mined by 1P as the candidate locations, the optimization process of 2P was conducted in discrete space. However, 3P could further

adjust the newly-built metering stations to the optimal location in the continuous space, thereby shortening the length of the newly-built pipelines. As shown in Fig. 7 and Table 3, under the economic goal, when potential locations were mined in 1P, the number of newly-built metering stations in 2P was the same as that in 3P, but the length of new-built pipelines decreased from 38,086 to 36,236 m.

Finally, the potential locations mined by the proposed method

Table 4Basic parameters of old metering stations.

	Maximum connection number/The connection number	Maximum processing capacity/The fluid volume processed before	
stations	before optimization	optimization, m ³ /d	10 ³ ¥
[1]	9/7	1200/800	350
[2]	10/9	1230/1133	420
[3]	8/5	780/335	250
[4]	7/5	1300/635	380
[5]	5/5	900/548	280
[6]	9/6	1200/725	370
[7]	9/8	1200/954	350
[8]	9/5	1080/602	290
[9]	8/5	1200/516	360
[10]	9/6	1400/814	410

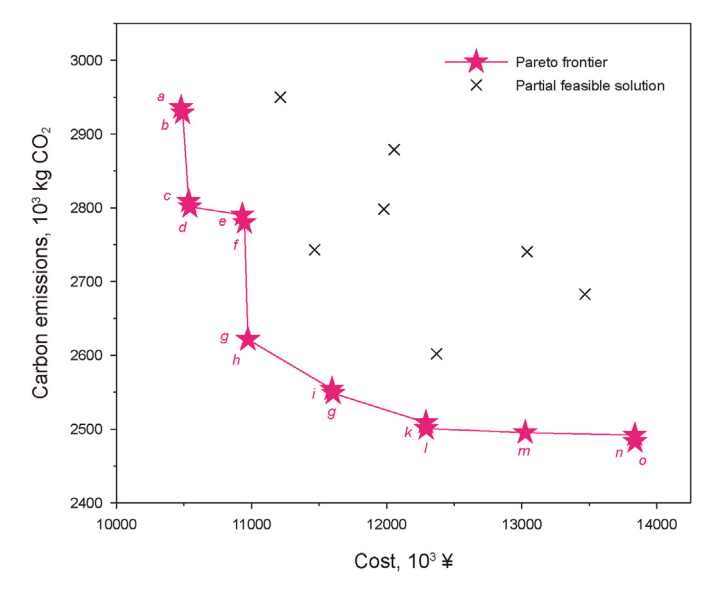


Fig. 9. Pareto frontier of case 2.

proved superior to those generated in grid and random forms. For example, under the economic goal, when potential locations were mined in 1P, the cost optimization ratios of 2P (vs. no 1P) (9.15%), 3P (vs. no 1P) (10.45%), 3P (vs. 2P) (2.25%) were the highest among all methods. In addition, although the numbers of potential locations generated in the grid and random forms were more than twice that mined in 1P, the costs of the latter were less than those of the former. The above phenomena indicated that the 3-phase heuristic model performed well in new blocks.

4.2. Case 2: an old oilfield

Fig. 8 shows the construction plan of an old oilfield in the late stage, which includes 58 old wells, 48 new wells, 3 abandoned wells, and 10 old metering stations. The basic parameters of the old metering stations are shown in Table 4, and the maximum connection number and processing capacity of the newly-built metering station are 10, 1400 m³/d, respectively.

As shown in Fig. 9, there are 15 Pareto frontier points in this case, where point a corresponds to the reconstruction scheme under the economic optimum and point o corresponds to the reconstruction scheme under the environmental optimum.

The optimization process under the economic goal is shown in Fig. 10. As shown in Fig. 10(a), in 1P, six potential locations were mined, five of which were left in 2P, and one was abandoned in 2P,

resulting in a selection ratio of potential locations being 83.3%. 3P underwent two iterations. As shown in Fig. 10(a) and (b), in the first iteration, all five new metering stations moved significantly in S1, and the connection relationships of W101 and W95 were changed in S2. As shown in Fig. 10(c), in the second iteration, only the metering stations [14] and [15] were adjusted. Additionally, the final reconstruction plan involved the recycling operations, as detailed in Table 5 and Fig. 10. Specifically, one old metering station and twelve pipelines, nine of which were connected to old wells and three to abandoned wells, were recycled, yielding 582,573 ¥ and emitting 13,642 kg CO₂e. The final topology and pipeline specifications are shown in Fig. 2 and Table S7, Section S5.2.

The constraints directly influence the development of the optimization scheme. As shown in Fig. 10(d), the new well W69 was connected to metering station [2]. Suppose no wells were disconnected from metering station [2], its processing rate would reach 1280 m³/d, exceeding its maximum processing capacity (1230 m³/ d, Table 4). Thus, under the constraints of Eq. (31), the old well W11 was assigned from metering station [2] to metering station [1]. Moreover, all wells met the gathering radius constraints to ensure the transportation of production fluids through gathering pipelines to metering stations. For example, under the constraints of Eq. (27) and economic consideration, the new well W86 was connected to metering station [13], which was within the gathering radius, rather than being connected to metering stations [12], [14], or others. Additionally, Eqs. (22) and (23) also served as constraints. Taking the old metering station [9] as an example, the known 0-1variable $P_m^{\rm b}$ for this station was set to 1. Under the economic objective, the 0-1 decision variables for this station were determined as $P_m^{\rm n}=0$, $P_m^{\rm c}=1$, and $P_m^{\rm s}=0$. It can be observed that these known and decision variables satisfied the constraints of Eqs. (22) and (23). Finally, the known 0–1 variable $\mu_i^{\rm no}$ for the abandoned wells was set to 0, while $\mu_i^{\text{no}} = 1$ for both old and new wells. Under the constraint of Eq. (26), all gathering pipelines connected to the abandoned wells were recycled, while each old well and new well was connected to a metering station.

As shown in Fig. 11(a) and (b), the load ratio and connection ratio of the old metering station rose dramatically after optimization, with the average load ratio increasing from 60.8% to 89.7% and the connection ratio increasing from 74.2% to 94.9%. These results indicated that the 3-phase heuristic model effectively enhanced the resource utilization of the old oilfield. As shown in Fig. 11(c), the average load ratio of the new metering station was 77.1%, and the average connection ratio was 70.0%. The lower load ratio and connection ratio of the newly-built metering station could be attributed to the lower well density in the new block. As more infill wells are drilled in the new block in the future, the load ratio and connection ratio of the newly-built metering station will gradually

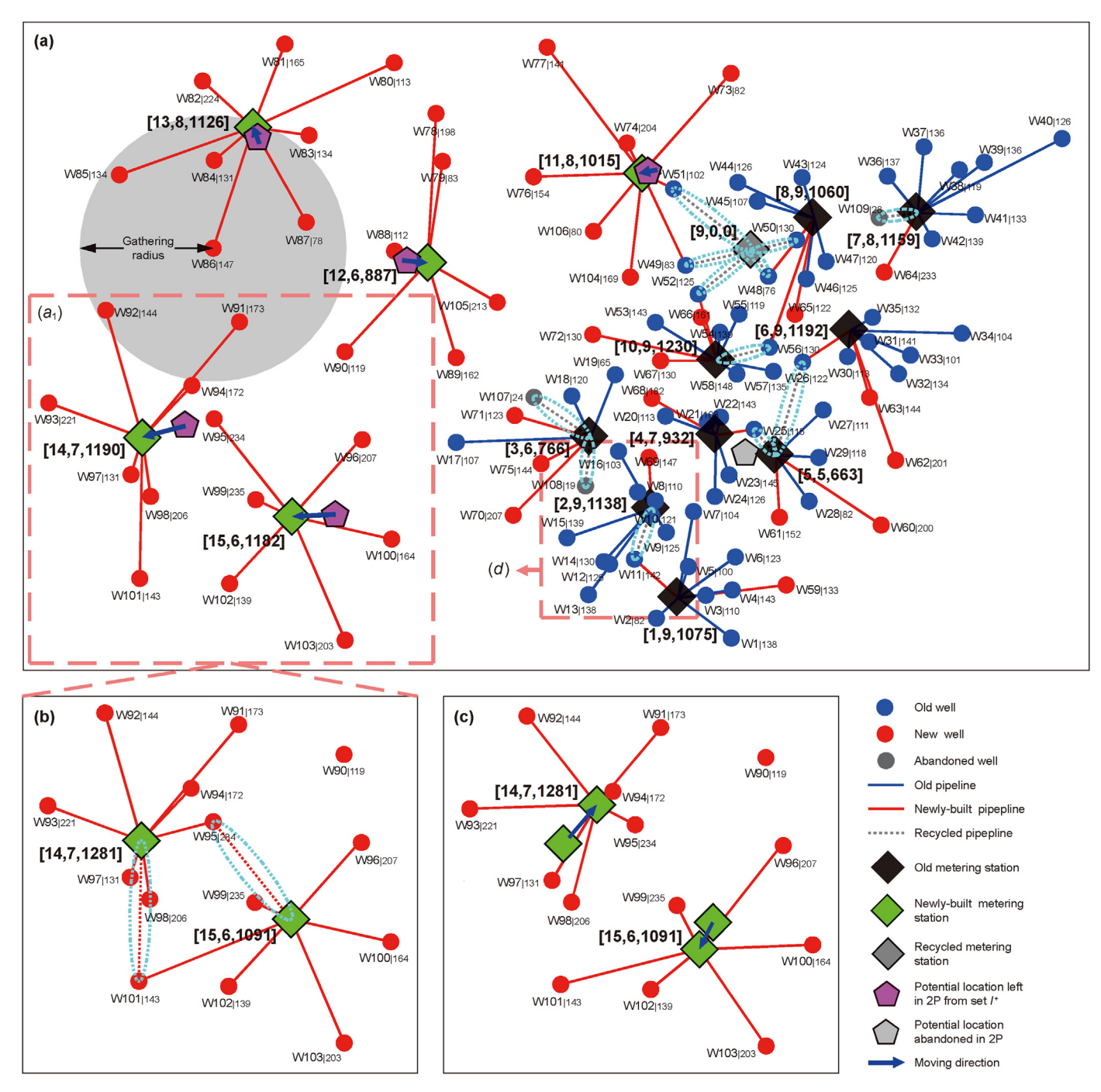


Fig. 10. The optimization processes of (a) 1P, 2P, and (b-c) 3P under the economic goal.

increase.

Table 6 shows the optimal results with different methods. Similar to case 1, under the economic goal, when the potential locations of the newly-built metering station were mined in 1P, the economic indicators were the best among several methods, indicating that the 3-phase heuristic model had an excellent performance in reconstructing old oilfields. For example, the cost of generating potential locations in 1P was 10,479,060 ¥, which was 9.48% lower than the cost (11,577,075 ¥) without generating potential locations. As for the carbon emissions, sacrificing 32.20% (vs. economic goal) of the cost could lead to the environmental optimum. Under the environmentally optimal conditions, the total

carbon emissions were 2,483,120 kg CO_2e , which was 8.84% lower than that under the economic goal without generating potential locations (2,724,085 kg CO_2e).

4.3. Sensitivity analysis

Wellhead pressure and temperature during the design phase are obtained through reservoir simulations. However, uncertainties in reservoir parameters, such as porosity and permeability, often result in discrepancies between the gathering radius during the design phase and that during the operation phase (Silva and Guedes Soares, 2021). Additionally, unpredictable factors like rainfall

Table 5Profit and carbon emissions of recycling.

Connection		Specification	Length, m	Recycling profit, ¥	Carbon emissions, kg CO2e
Old pipelines connected to old wells	W11-[2]	III	477	20320	1067
	W25-[5]	II	304	10944	516
	W26-[5]	II	869	31284	1472
	W48-[9]	I	272	8650	399
	W49-[9]	I	610	19398	893
	W50-[9]	II	411	14796	696
	W51-[9]	II	895	32220	1516
	W52-[9]	II	619	22284	1049
	W56-[10]	II	487	17532	825
Old pipelines connected to recycled wells	W107-[3]	I	629	20002	912
	W108-[3]	I	442	14056	641
	W109-[7]	I	348	11066	505
Old metering station		[9]		360000	3152
Total recycling profit, ¥	582573	Total carbon emissions, kg CO ₂ e		13642	

Table 6Optimal results with different methods.

		Without generating potential location (no 1P) Economic goal			Environmental goal	
			Generating	potential location	In 1P	
			In 1P	In the random	In the grid	
1P	Number of intersection points Number of newly-built metering stations Number of potential locations mined in 1P	 	3250 6 6	/ / 16	/ / 16	3250 10 6
2P	Cost, ¥ Carbon emissions, kg CO ₂ e	11,638,899 2,750,264	10,703,443 3,040,612	11,040,303 2,835,759	11,638,899 2,750,264	13,866,761 2,492,798
3P	Number of newly-built metering stations Number of reserved metering stations Number of recycled metering stations Cost, ¥ Carbon emissions, kg CO ₂ e	7 9 1 11,577,075 2,724,085	5 9 1 10,479,060 2,935,971	6 9 1 10,989,928 2,814,115	7 9 1 11,577,075 2,724,085	10 10 0 13,839,029 2,483,120
Cost optimization ratio of 2P (vs. no 1P), % Cost optimization ratio of 3P (vs. no 1P), % Cost optimization ratio of 3P (vs. 2P), %		0.53	8.07 9.48 2.14	5.16 5.07 0.46	0 0 0.53	-29.68 (vs. economic goal) -32.20 (vs. economic goal) 0.20

during construction may lead to project delays and increase the pipeline construction cost. Conversely, advancements in pipe manufacturing processes reduce manufacturing costs. Furthermore, the maximum connection number and processing capacity varies among different types of metering stations. Overall, it can be found that the external conditions of OGGS are dynamically changing.

In this section, sensitivity analysis was conducted to assess the impact of the aforementioned parameters on the reconstruction scheme. With the economy as the objective, the proposed method generated optimized reconstruction schemes for case 2. Due to variations in gathering radius among wells and differences in pipeline construction cost per unit length among pipeline specifications, the factors of gathering radius and pipeline construction cost were introduced. These factors refer to the ratio of the gathering radius to the unit gathering radius and the ratio of pipeline construction cost per unit length to unit cost, respectively. The unit gathering radius denotes the gathering radius of the well during the design phase, and the unit cost denotes the current pipeline construction cost per unit length.

4.3.1. The gathering radius

The shorter the gathering radius was, the more significant the influence of the gathering radius on the reconstruction scheme was. Specifically, as shown in Fig. 12, with the increase in gathering radius, the total cost and total carbon emissions initially decreased

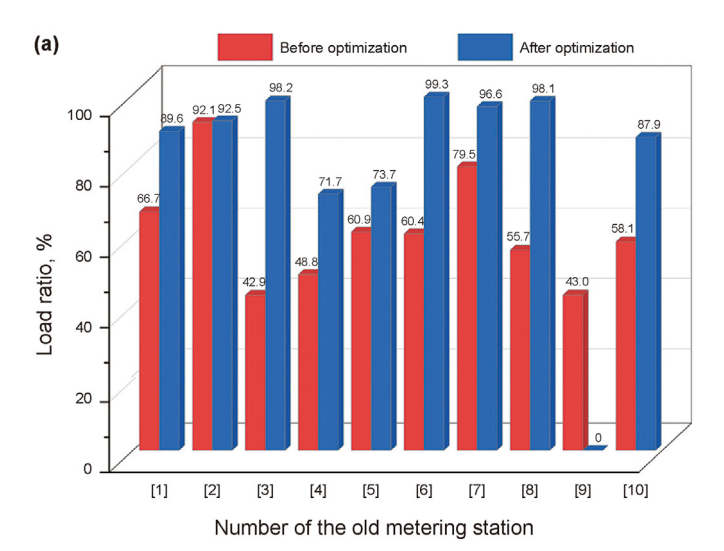
sharply, followed by a gradual stabilization. Additionally, as the gathering radius increased, a decreasing trend was observed in the number of newly-built metering stations, accompanied by an increasing trend in the length of newly-built pipeline. The total cost and carbon emissions exhibited a similar trend to the number of newly-built metering stations, implying that the number of newly-built metering stations was the primary factor affecting the economic and low carbon indicators of the reconstruction scheme.

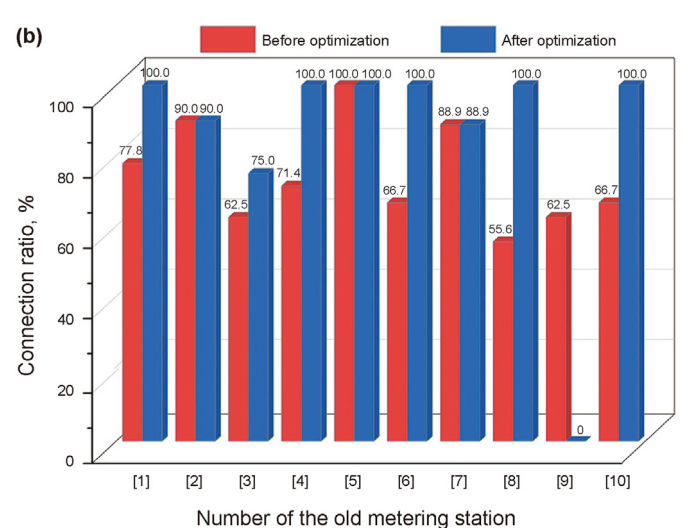
4.3.2. The pipeline construction cost per unit length

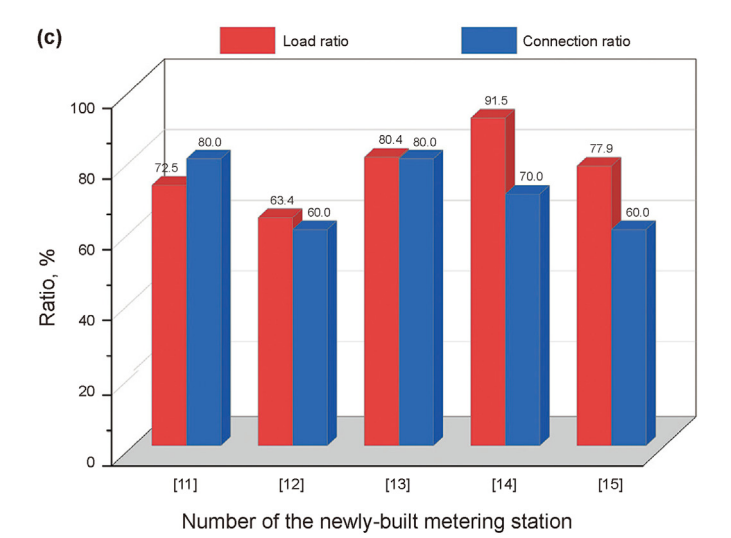
As shown in Fig. 13(a), the increase in pipeline construction cost per unit length led to an increase in the number of newly-built metering stations and a reduction in the length of newly-built pipeline. In addition, since 1P was unaffected by the pipeline construction cost per unit length, the number of potential locations mined in 1P remained unchanged. The above two phenomena were the main reasons for the decrease in the selection ratio of potential locations when the factor of pipeline construction cost was 1.6, 2.3, 3.2, and 3.6. As shown in Fig. 13(b), the total cost increased linearly with the pipeline construction cost per unit length.

4.3.3. The maximum connection number and processing capacity of the newly-built metering station

The sensitivity of the maximum connection number and processing capacity is shown in Fig. 14, where <a, b, c> denotes < maximum connection number, maximum processing







Note: ① Load ratio = Actual fluid volume processed + Maximum processing capacity × 100%;
② Connection ratio = Actual connection number + Maximum connection number × 100%

Fig. 11. The load ratio and connection ratio of metering stations.

capacity, optimization result>. The following discussion was based on a fixed maximum connection number (10) to reveal the sensitivity of the maximum processing capacity. When the processing capacity was raised from 400 to 1000 m³/d, the number of newlybuilt metering stations dropped from 19 to 6, and the total cost dropped from 23,187,493 to 11,184,484 $\mbox{\normalfont 4}$, resulting in a 51.7% reduction in total cost. However, all parameters stabilized when the maximum processing capacity further increased. For instance, when the processing capacity exceeded 1300 m³/d, the total cost and carbon emissions remained unchanged at 10,479,060 $\mbox{\normalfont 4}$ and 2,935,971 kg CO₂e, respectively. Therefore, it can be inferred that there was a margin for the maximum processing capacity of the newly-built metering station.

The maximum connection number had a similar impact on the reconstruction scheme as the maximum processing capacity, and a margin for the maximum connection number was also identified. Specifically, when the number of metering stations exceeded 8, there were no changes in the number of newly-built metering stations, the length of newly-built pipelines, the total cost, and the total carbon emissions. In summary, for case 2, the maximum processing capacity and connection number of the newly-built metering station could be adjusted from 1400 to 1300 m³/d and from 10 to 8, respectively, i.e., moving point *D* to point *C*, improving the load ratio of the OGGS.

5. Discussions

Based on the case studies and sensitivity analyses, several meaningful results that could provide recommendations were presented and worth discussing in this section.

In previous pipeline network design optimization, station facilities (e.g., metering stations) were generally co-located with existing facilities (e.g., wells), so previous optimization efforts were operated in discrete space (Üster and Dilaveroğlu, 2014; Liu et al., 2019; Hong et al., 2020; Zhou et al., 2021, 2024). Differently, considering the process characteristics of the OGGS, the potential locations were mined in continuous space in this study. In case 1, the study achieved a maximum cost reduction of 10.45% and a maximum carbon reduction of 7.21%. Thus, conducting reconstruction optimization in discrete space no longer meets the economic and low-carbon development of the OGGS, and the decisionmaker should shift their attention from discrete to continuous space to further mine high-quality potential locations. Meanwhile, although this study focused on the "well-to-metering station", it also provided a reference for on-site designers to explore highquality construction locations for the transfer station and CPF in continuous space.

Optimization studies on the new pipeline network design, and multi-period network construction have been widely conducted (Ramos Rosa et al., 2018; Hong et al., 2020; Wu et al., 2022; Yue et al., 2023; Liu et al., 2024). However, these studies often focus on constructing new facilities and overlook the recycling of old ones. In case 2, the recycling measure was applied to an old oilfield, and one low-load metering station and twelve pipelines were recycled, yielding a profit of 582,573 ¥, which accounted for 5.56% of the total cost. Therefore, decision-makers can integrate recycling with new construction to diversify oilfield reconstruction strategies. This approach not only reduces reconstruction cost but also lowers operation cost by improving the load ratio of the facilities.

The sensitivity analysis revealed that the gathering radius obviously impacted the optimization scheme, particularly when the gathering radius was limited. Generally, in old and low-permeability oilfields, insufficient formation energy often results in a smaller gathering radius (Jiang et al., 2024), so on-site



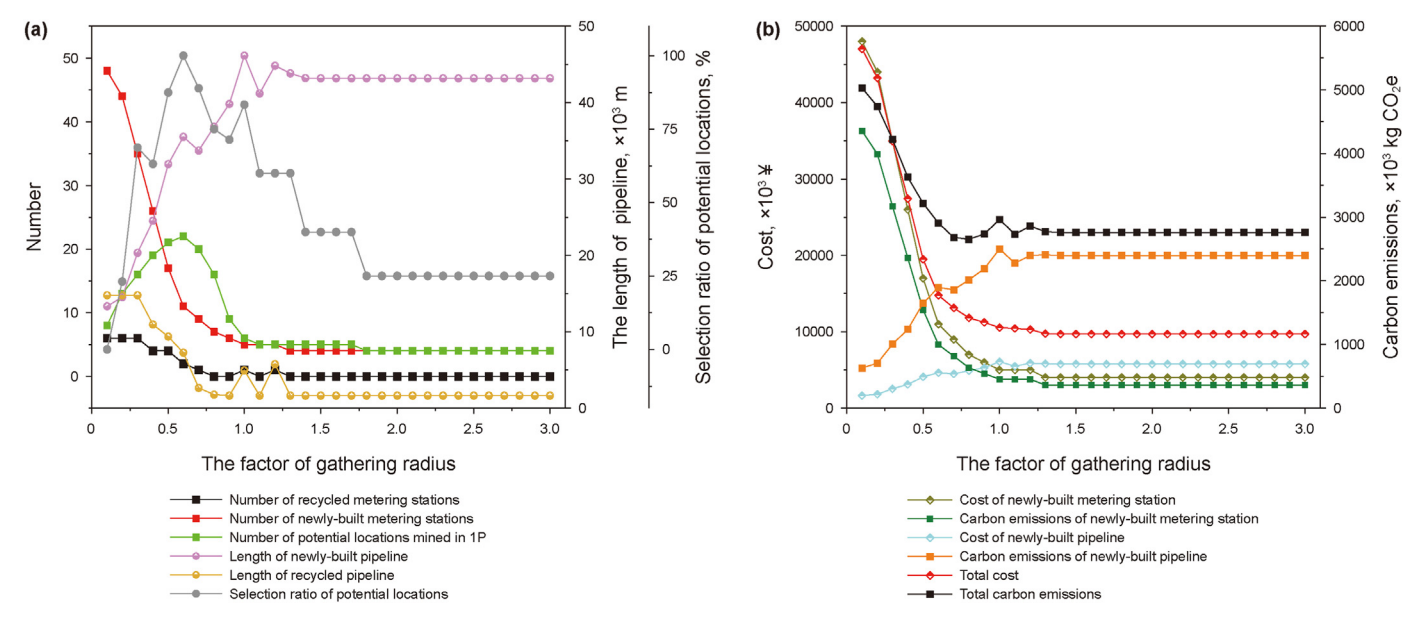


Fig. 12. Sensitivity analysis of the gathering radius.

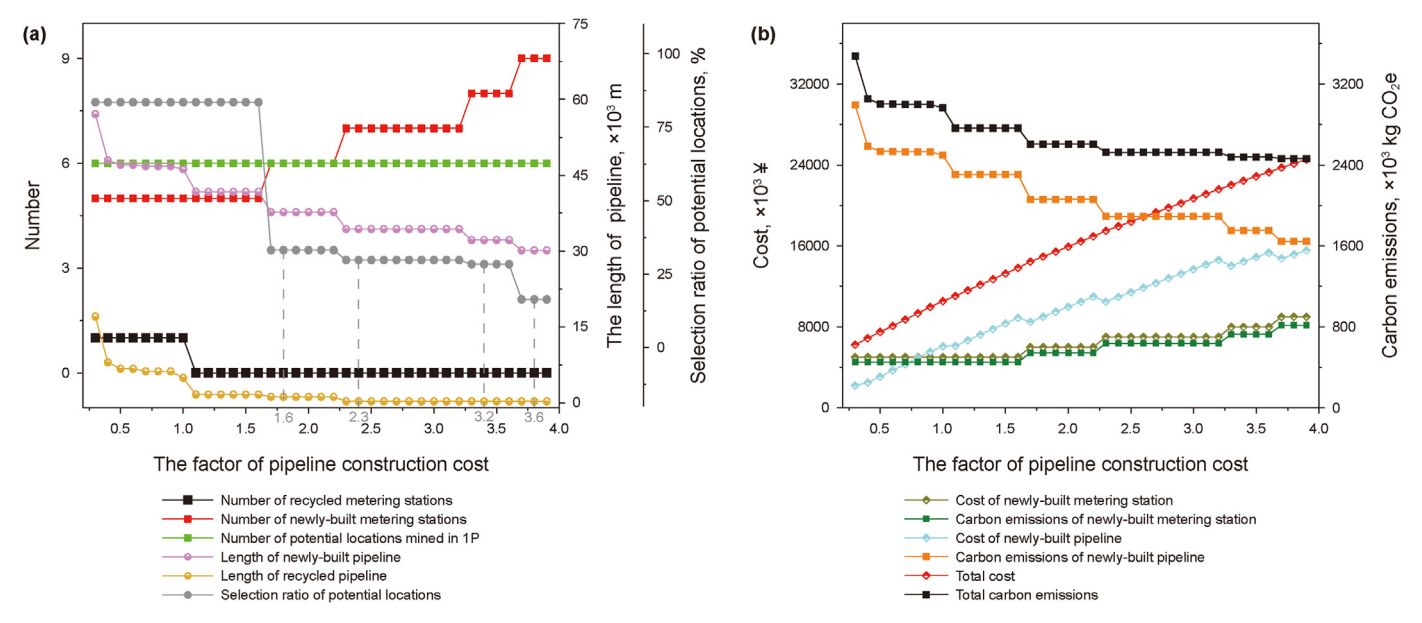


Fig. 13. Sensitivity analysis of the pipeline construction cost per unit length.

designers should accurately simulate the gathering radius of wells during the design stage. Underestimating the gathering radius may lead to a sharp increase in the reconstruction cost and carbon emissions. Subsequently, the sensitivity analysis showed that as the pipeline construction cost per unit length declined, the number of newly-built metering stations decreased while the selection ratio of potential locations rose. Therefore, it is necessary for decision-makers to introduce new technologies to reduce the pipeline construction cost.

Finally, as shown in Fig. 14, when the maximum connection number and processing capacity were limited, there was a significant decrease in total cost and carbon emissions with increasing maximum connection number and processing capacity. However, in case 2, once the maximum connection number exceeded 8 and the maximum processing capacity exceeded 1300 m³/d, the total

cost and carbon emissions stabilized. Therefore, on-site designers should put sufficient effort into selecting the appropriate type of metering station during the design phase, such as the multi-factor analysis. This approach prevents high construction cost and carbon emissions during the construction phase due to insufficient connection number and processing capacity, as well as avoids the low load ratio during the operation phase caused by excessive connection number and processing capacity.

6. Conclusions

In response to the demand for the reconstruction of OGGS, guided by sustainable development, this study developed a 3-phase heuristic model based on potential location mining in continuous space to evaluate the carbon emissions and cost during

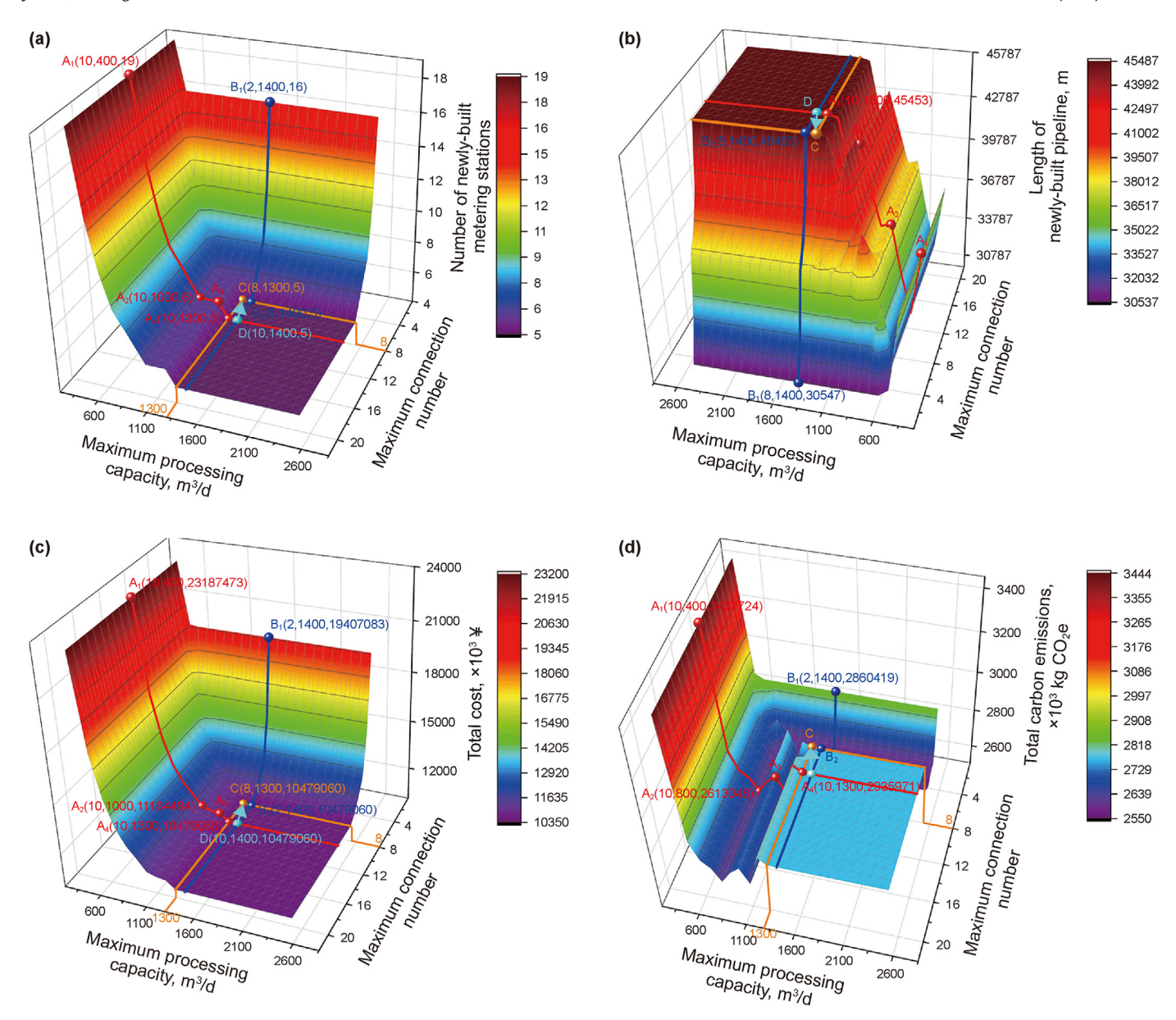


Fig. 14. Sensitivity analysis of maximum connection number and processing capacity of the newly-built metering station: (a) the number of newly-built metering stations, (b) the length of newly-built pipeline, (c) total cost, and (d) total carbon emissions.

the reconstruction phase. Numerical experiments demonstrated the superiority and applicability of the proposed model. The results showed that a small number of potential locations could effectively reduce the reconstruction cost. Moreover, the high quality of potential locations mined in 1P was evidenced by the higher selection ratio of potential locations compared to those generated in random and grid form.

Case studies revealed that the proposed model performed well in both new blocks and old oilfields. In case 1, the proposed model reduced the cost by up to 10.45% and carbon emissions by up to 7.21% compared to the baseline case. These improvements were attributed to the fact that the potential locations mined in 1P reduced the number of metering stations, and the modified Cooper's algorithm in 3P optimized the locations of metering stations in continuous space to shorten the pipeline length. For the old oilfield reconstruction, the economic indicators were best when potential locations were mined in 1P, compared to random and grid

forms. Additionally, introducing the recycling measure led to the recovery of one metering station and twelve pipelines, yielding a profit equivalent to 5.56% of the total cost. Lastly, the average load ratio of old metering stations increased from 60.8% to 89.7%, and the average connection ratio of old metering stations increased from 74.2% to 94.9%, indicating an improvement in resource utilization of the old oilfield.

Sensitivity analysis indicated that the reconstruction cost and carbon emissions were highly sensitive to the low gathering radius, so on-site designers should prioritize evaluating the gathering radius for the oilfields with low gathering radius. Moreover, the low pipeline construction cost could increase the selection ratio of potential locations, thereby enhancing the optimization effectiveness of the proposed model. Furthermore, sensitivity analysis suggested that there was a margin to reduce the maximum connection number and processing capacity of the newly-built metering station to 8 and 1300 $\rm m^3/d$ in case 2, respectively. This

adjustment could improve the load ratio of metering stations, promoting the economic and low-carbon operation of the OGGS.

The economic and carbon reduction potentials were tapped in continuous space for oilfield reconstruction in this study, which serves as a reference valuable for developing economic and low-carbon reconstruction plans for oilfields. Further research could be conducted based on this study. Over time, the compatibility between the reconstruction design scheme and the actual operation status of the OGGS will inevitably decrease. Thus, an operation optimization model for the OGGS should be developed to adjust the flow directions and equipment operation schemes, improving the operation efficiency. Additionally, this study primarily focused on the OGGS. Since the operation status of the water injection network influences that of the OGGS through the reservoir, it remains a challenge to conduct reconstruction optimization research on "injection system—reservoir-OGGS" for the integrated management of oilfields.

CRediT authorship contribution statement

Jie Chen: Writing — original draft, Validation, Software, Methodology, Formal analysis, Conceptualization. **Wei Wang:** Supervision, Methodology, Funding acquisition, Conceptualization. **Wen-Yuan Sun:** Writing — review & editing, Investigation, Data curation. **Dong Li:** Visualization, Validation. **Yu-Bo Jiao:** Visualization, Data curation.

Declaration of competing interest

The authors declare that they have no known competing financial interests or personal relationships that could have appeared to influence the work reported in this paper.

Acknowledgments

This work was partially supported by the National Natural Science Foundation of China (Grant No. 52174065), the National Natural Science Foundation of China (Grant No. 52304071), China University of Petroleum, Beijing (Grant No. ZX20220040), and MOE Key Laboratory of Petroleum Engineering (China University of Petroleum, No. 2462024PTJS002).

Appendix A. Supplementary data

Supplementary data to this article can be found online at https://doi.org/10.1016/j.petsci.2024.12.011.

References

- Allen, A., Henze, G., Baker, K., Pavlak, G., Murphy, M., 2022. An optimization framework for the network design of advanced district thermal energy systems. Energy Convers. Manag. 266, 115839. https://doi.org/10.1016/ j.enconman.2022.115839.
- Alves, F.d.S., Souza, J.N.M.d., Costa, A.L.H., 2016. Multi-objective design optimization of natural gas transmission networks. Comput. Chem. Eng. 93, 212–220. https://doi.org/10.1016/j.compchemeng.2016.06.006.
- Bai, Y.J., Hou, J., Liu, Y.G., Zhao, D., Bing, S.X., Xiao, W., Zhao, W., 2022. Energy-consumption calculation and optimization method of integrated system of injection-reservoir-production in high water-cut reservoir. Energy 239, 121961. https://doi.org/10.1016/j.energy.2021.121961.
- Chen, J., Wang, W., Sun, W.Y., Jiao, Y.B., He, Y.M., Li, D., Gong, J., 2023. Tapping into the potential CO2 emission reduction of a crude oil transportation system from carbon footprint perspective. J. Clean. Prod. 413, 137409. https://doi.org/10.1016/ i.jclepro.2023.137409.
- Cooper, L., 1964. Heuristic methods for location-allocation problems. SIAM Rev. 6 (1), 37–53. https://doi.org/10.1137/1006005.
- Dbouk, H.M., Hayek, H., Ghorayeb, K., 2021. Modular approach for optimal pipeline layout. J. Pet. Sci. Eng. 197, 107934. https://doi.org/10.1016/j.petrol.2020.107934.
- Denat, T., Harutyunyan, A., Melissinos, N., Paschos, V.T., 2024. Average-case complexity of a branch-and-bound algorithm for min dominating set. Discrete

Appl. Math. 345, 4-8. https://doi.org/10.1016/j.dam.2023.11.021.

- Feng, Q.H., Li, S.S., Zhang, X.M., Gao, X.F., Ni, J.H., 2022. Well production optimization using streamline features-based objective function and Bayesian adaptive direct search algorithm. Petrol. Sci. 19 (6), 2879—2894. https://doi.org/10.1016/j.petsci.2022.06.016.
- He, G.X., Chen, D., Liao, K.X., Sun, J.F., Nie, S.M., 2019. A methodology for the optimal design of gathering pipeline system in old oilfield during its phased development process. Comput. Ind. Eng. 130, 14–34. https://doi.org/10.1016/j.cie.2019.02.016.
- Hong, B.Y., Li, X.P., Di, G.J., Li, Y., Liu, X.S., Chen, S.L., Gong, J., 2019. An integrated MILP method for gathering pipeline networks considering hydraulic characteristics. Chem. Eng. Res. Des. 152, 320–335. https://doi.org/10.1016/ j.cherd.2019.08.013.
- Hong, B.Y., Li, X.P., Di, G.J., Song, S.F., Yu, W.C., Chen, S.L., Li, Y., Gong, J., 2020. An integrated MILP model for optimal planning of multi-period onshore gas field gathering pipeline system. Comput. Ind. Eng. 146, 106479. https://doi.org/10.1016/j.cie.2020.106479.
- Huang, L.Q., Liao, Q., Yan, J.Y., Liang, Y.T., Zhang, H.R., 2021. Carbon footprint of oil products pipeline transportation. Sci. Total Environ. 783, 146906. https://doi.org/10.1016/j.scitotenv.2021.146906.
- Huang, Z.Q., Wang, Z.X., Hu, H.F., Zhang, S.M., Liang, Y.X., Guo, Q., Yao, J., 2023. Dynamic interwell connectivity analysis of multi-layer waterflooding reservoirs based on an improved graph neural network. Petrol. Sci. 21 (2), 1062–1080. https://doi.org/10.1016/j.petsci.2023.11.008.
- Iglesias-Rey, P.L., Martínez-Solano, F.J., Saldarriaga, J.G., Navarro-Planas, V.R., 2017. Pseudo-genetic Model optimization for rehabilitation of urban storm-water drainage networks. Procedia Eng. 186, 617–625. https://doi.org/10.1016/ j.proeng.2017.03.278.
- Ji, B.Y., Xu, T., Gao, X.J., Yu, H.M., Liu, H., 2023. Production evolution patterns and development stage division of waterflooding oilfields. Petrol. Explor. Dev. 50 (2), 433–441. https://doi.org/10.1016/s1876-3804(23)60398-2.
- Ji, L., Liu, Y.M., Guo, X.L., Wang, F., Zhang, R.J., Sun, J., Bao, L., 2021. Geological controlling factors of single well productivity in perforated and fractured reservoir in Zaoyuan oilfield. Pet. Sci. Bull. 6 (4), 566–575. https://doi.org/ 10.3969/j.issn.2096-1693.2021.04.039 (in Chinese).
- Jiang, H.Z., Yang, H.B., Pan, R.S., Ren, Z.Y., Kang, W.L., Zhang, J.Y., Pan, S.L., Sarsenbekuly, B., 2024. Performance and enhanced oil recovery efficiency of an acid-resistant polymer microspheres of anti-CO₂ channeling in lowpermeability reservoirs. Petrol. Sci. 21 (4), 2420–2432. https://doi.org/ 10.1016/j.petsci.2024.02.002.
- Liu, E.B., Peng, Y., Yi, Y., Lv, L.X., Qiao, W.B., Azimi, M., 2020. Research on the steady-state operation optimization technology of oil pipeline. Energy Sci. Eng. 8 (11), 4064–4081. https://doi.org/10.1002/ese3.795.
- Liu, S.T., Zhou, J., Liang, G.C., Du, P.H., Li, Z.C., Li, C.Y., 2024. Optimizing large-scale hydrogen storage: a novel hybrid genetic algorithm approach for efficient pipeline network design. Int. J. Hydrogen Energy 66, 430–444. https://doi.org/ 10.1016/j.ijhydene.2024.04.098.
- Liu, Y., Chen, S.Q., Guan, B., Xu, P., 2019. Layout optimization of large-scale oil—gas gathering system based on combined optimization strategy. Neurocomputing 332, 159–183. https://doi.org/10.1016/j.neucom.2018.12.021.
- Liu, Y., Li, J.X., Wang, Z.H., Wang, S.Z., Dong, Y.C., 2015. The role of surface and subsurface integration in the development of a high-pressure and lowproduction gas field. Environ. Earth Sci. 73 (10), 5891–5904. https://doi.org/ 10.1007/s12665-015-4341-7.
- Malallah, A., Alashwak, A., Nashawi, I.S., 2021. Infill well placement optimization in two-dimensional heterogeneous reservoirs under waterflooding using upscaling wavelet transform. J. Pet. Sci. Eng. 201, 108439. https://doi.org/10.1016/ j.petrol.2021.108439.
- Mavrotas, G., 2009. Effective implementation of the ε-constraint method in multiobjective mathematical programming problems. Appl. Math. Comput. 213 (2), 455–465. https://doi.org/10.1016/j.amc.2009.03.037.
- Mavrotas, G., Florios, K., 2013. An improved version of the augmented ε-constraint method (AUGMECON2) for finding the exact pareto set in multi-objective integer programming problems. Appl. Math. Comput. 219 (18), 9652–9669. https://doi.org/10.1016/j.amc.2013.03.002.
- Neumann, C., Schwarze, S., Stein, O., Müller, B., 2022. Feasible rounding based diving strategies in branch-and-bound methods for mixed-integer optimization. EURO J. Comput. Optim. 10, 100051. https://doi.org/10.1016/ i.ejco.2022.100051.
- Rahmawati, S.D., Whitson, C.H., Foss, B., Kuntadi, A., 2012. Integrated field operation and optimization. J. Pet. Sci. Eng. 81, 161–170. https://doi.org/10.1016/ j.petrol.2011.12.027.
- Ramos Rosa, V., Camponogara, E., Martins Ferreira Filho, V.J., 2018. Design optimization of oilfield subsea infrastructures with manifold placement and pipeline layout. Comput. Chem. Eng. 108, 163–178. https://doi.org/10.1016/j.compchemeng.2017.08.009.
- Sánchez, D.G., Tabares, A., Faria, L.T., Rivera, J.C., Franco, J.F., 2022. A clustering approach for the optimal siting of recharging stations in the electric vehicle routing problem with time windows. Energies 15 (7), 2372. https://doi.org/ 10.3390/en15072372.
- Shin, H., Joo, C., Koo, J., 2016. Optimal rehabilitation model for water pipeline systems with genetic algorithm. Procedia Eng. 154, 384–390. https://doi.org/10.1016/j.proeng.2016.07.497.
- Silva, L.M.R., Guedes Soares, C., 2019. An integrated optimization of the floating and subsea layouts. Ocean Eng. 191, 106557. https://doi.org/10.1016/

j.oceaneng.2019.106557.

- Silva, L.M.R., Guedes Soares, C., 2021. Oilfield development system optimization under reservoir production uncertainty. Ocean Eng. 225, 108758. https:// doi.org/10.1016/j.oceaneng.2021.108758.
- Song, Z.J., Li, Z.P., Lai, F.P., Liu, G., Gan, H.H., 2013. Derivation of water flooding characteristic curve for high water-cut oilfields. Petrol. Explor. Dev. 40 (2), 216–223. https://doi.org/10.1016/s1876-3804(13)60025-7.
- Sun, L.D., Jiang, T.W., Wang, F.L., Wu, X.L., Luo, K., Jiang, H., Han, P.H., 2021. Thoughts on the development life of oilfield. Acta Pet. Sin. 42 (1), 56–63. https://doi.org/ 10.7623/syxb202101005 (in Chinese).
- Taheri, N., Pishvaee, M.S., 2024. A regret-based robust optimization model for municipal water distribution network redesign under disruption risks. Comput. Chem. Eng. 185, 108676. https://doi.org/10.1016/j.compchemeng.2024.108676.
- Tang, X., Li, Y.L., 2023. Towards a zero-carbon future: a literature review of carbon emission accounting and management. Pet. Sci. Bull. 8 (4), 522–534. https://doi.org/10.3969/j.issn.2096-1693.2023.04.040 (in Chinese).
- Tomazella, C.P., Nagano, M.S., 2020. A comprehensive review of Branch-and-Bound algorithms: guidelines and directions for further research on the flowshop scheduling problem. Expert Syst. Appl. 158, 113556. https://doi.org/10.1016/ i.eswa.2020.113556.
- Üster, H., Dilaveroğlu, Ş., 2014. Optimization for design and operation of natural gas transmission networks. Appl. Energy 133, 56–69. https://doi.org/10.1016/j.apenergy.2014.06.042.
- Vardi, Y., Zhang, C.H., 2001. A modified Weiszfeld algorithm for the Fermat-Weber location problem. Math. Program. 90, 559–566. https://doi.org/10.1007/ s101070100222.
- Wang, B.H., Liang, Y.T., Yuan, M., Wang, J.H., Zhang, H.R., Li, X.J., 2018a. Optimal design of oilfield surface pipeline networks for the cyclic water injection development method. J. Pet. Sci. Eng. 171, 1400—1408. https://doi.org/10.1016/ j.petrol.2018.08.065.
- Wang, B.H., Liang, Y.T., Zheng, J.Q., Lei, T.T., Yuan, M., Zhang, H.R., 2018b. A methodology to restructure a pipeline system for an oilfield in the mid to late stages of development. Comput. Chem. Eng. 115, 133–140. https://doi.org/ 10.1016/j.compchemeng.2018.04.008.
- Wang, B.H., Yuan, M., Zhang, H.R., Zhao, W.J., Liang, Y.T., 2018c. An MILP model for optimal design of multi-period natural gas transmission network. Chem. Eng. Res. Des. 129, 122—131. https://doi.org/10.1016/j.cherd.2017.11.001.
- Wang, Y., Wang, Q., Zhang, A.X., Qiu, W.W., Duan, M.L., Wang, Q.S., 2021. A new optimization algorithm for the layout design of a subsea production system. Ocean Eng. 232, 109072. https://doi.org/10.1016/j.oceaneng.2021.109072.
- Wang, Y.X., Yang, Z.X., Yin, X.J., Zhu, Q.S., Lian, J.G., 2022. Research on oilfield production forecasting technology under low-carbon background. Energy Rep. 8, 28–37. https://doi.org/10.1016/j.egyr.2022.05.083.
- Wang, Y.Y., Duan, M.L., Xu, M.H., Wang, D.G., Feng, W., 2012. A mathematical model for subsea wells partition in the layout of cluster manifolds. Appl. Ocean Res. 36, 26–35. https://doi.org/10.1016/j.apor.2012.02.002.
- Watanabe, A., Tamura, R., Takano, Y., Miyashiro, R., 2023. Branch-and-bound algorithm for optimal sparse canonical correlation analysis. Expert Syst. Appl. 217,

119530. https://doi.org/10.1016/j.eswa.2023.119530.

- Weiszfeld, E., Plastria, F., 2008. On the point for which the sum of the distances to n given points is minimum. Ann. Oper. Res. 167 (1), 7–41. https://doi.org/10.1007/s10479-008-0352-z.
- Wu, Y., Cui, Z.Y., Lin, H., Wang, Y.F., Feng, X., 2022. An optimization method for shale gas gathering system consideration of reliability enhancement under earthquake-related uncertainties. Petrol. Sci. 19 (5), 2431–2447. https://doi.org/10.1016/j.petsci.2021.12.029.
- Xu, S.Y., Wang, J.A., Sun, H., Huang, L.Q., Xu, N., Liang, Y.T., 2022. Life cycle assessment of carbon emission from natural gas pipelines. Chem. Eng. Res. Des. 185, 267–280. https://doi.org/10.1016/i.cherd.2022.07.018.
- Yan, S., Ji, X.Y., Fang, Y.J., Sun, H.G., 2021. Multiobjective multistage robust integer optimization model and algorithm for oilfield development planning. Comput. Ind. Eng. 159, 107497. https://doi.org/10.1016/j.cie.2021.107497.
- Yuan, S.Y., Wang, Q., 2018. New progress and prospect of oilfields development technologies in China. Petrol. Explor. Dev+. 45 (4), 698-711. https://doi.org/ 10.1016/s1876-3804(18)30073-9.
- Yue, Y.L., Li, Y.H., Zuo, X., 2023. Optimization of subsea production control system layout considering hydraulic fluid pressure loss. Ocean Eng. 288, 116047. https://doi.org/10.1016/j.oceaneng.2023.116047.
- Zhang, H.R., Liang, Y.T., Zhang, W., Wang, B.H., Yan, X.H., Liao, Q., 2017. A unified MILP model for topological structure of production well gathering pipeline network. J. Pet. Sci. Eng. 152, 284–293. https://doi.org/10.1016/j.petrol.2017.03.016.
- Zhang, L., Dou, H.E., Wang, T.Z., Wang, H.L., Peng, Y., Zhang, J.F., Liu, Z.S., Mi, L., Jiang, L.W., 2022. A production prediction method of single well in water flooding oilfield based on integrated temporal convolutional network model. Petrol. Explor. Dev. 49 (5), 1150–1160. https://doi.org/10.1016/s1876-3804(22) 60339-2.
- Zhang, X., Liao, Q., Wang, Q., Wang, L.M., Qiu, R., Liang, Y.T., Zhang, H.R., 2021. How to promote zero-carbon oilfield target? A technical-economic model to analyze the economic and environmental benefits of Recycle-CCS-EOR project. Energy 225, 120297. https://doi.org/10.1016/j.energy.2021.120297.
- Zhou, J., Fu, T.T., Chen, Y.L., Xiao, Y., Peng, J.H., Liang, G.C., 2021. A mixed integer nonlinear programming model for optimal design of natural gas storage surface double-pipe network. J. Energy Storage 44, 103379. https://doi.org/10.1016/ jest 2021.103379
- Zhou, J., Gong, J., Li, X.P., Tong, T., Cheng, M.Y., Zhang, S.Q., 2015. Optimization of coalbed methane gathering system in China. Adv. Mech. Eng. 6, 147381. https:// doi.org/10.1155/2014/147381.
- Zhou, J., Shi, Y., Liang, G.C., Peng, C., Liu, C., 2024. Mixed transportation optimization model for oilfield water injection synergizing pipeline network and trucks. Geoenergy Sci. Eng. 241, 213105. https://doi.org/10.1016/j.geoen.2024.213105.
- Zubail, A., Traidia, A., Masulli, M., Vatopoulos, K., Villette, T., Taie, I., 2021. Carbon and energy footprint of nonmetallic composite pipes in onshore oil and gas flowlines. J. Clean. Prod. 305, 127150. https://doi.org/10.1016/j.jclepro.2021.127150.